On the planar extensional motion of an inertially driven liquid sheet

Linda B. Smolka[1,a)] and Thomas P. Witelski[2,b)]
[1]*Department of Mathematics, Bucknell University, 380 Olin Science Building, Lewisburg, Pennsylvania 17837, USA*
[2]*Department of Mathematics, Duke University, Box 90320, Durham, North Carolina 27708, USA*

(Received 27 June 2008; accepted 5 February 2009; published online 7 April 2009)

We derive a time-dependent exact solution of the free surface problem for the Navier–Stokes equations that describes the planar extensional motion of a viscous sheet driven by inertia. The linear stability of the exact solution to one- and two-dimensional symmetric perturbations is examined in the inviscid and viscous limits within the framework of the long-wave or slender body approximation. Both transient growth and long-time asymptotic stability are considered. For one-dimensional perturbations in the axial direction, viscous and inviscid sheets are asymptotically marginally stable, though depending on the Reynolds and Weber numbers transient growth can have an important effect. For one-dimensional perturbations in the transverse direction, inviscid sheets are asymptotically unstable to perturbations of all wavelengths. For two-dimensional perturbations, inviscid sheets are unstable to perturbations of all wavelengths with the transient dynamics controlled by axial perturbations and the long-time dynamics controlled by transverse perturbations. The asymptotic stability of viscous sheets to one-dimensional transverse perturbations and to two-dimensional perturbations depends on the capillary number (Ca); in both cases, the sheet is unstable to long-wave transverse perturbations for any finite Ca. © *2009 American Institute of Physics*. [DOI: 10.1063/1.3094026]

I. INTRODUCTION

We consider the idealized free surface motion and stability of a Newtonian planar sheet extending in an inertially driven flow. Extensional flows appear in a wide variety of applications: in the rheological characterization of viscoelastic fluids,[1–4] in jets produced by shaped charges,[5,6] and in manufacturing processes, such as fiber drawing, fiber spinning, mixing processes, film blowing, and droplet formation.

The problem we examine is the planar analog of the uniaxial extensional motion of an inertially driven cylindrical jet or filament considered in previous studies.[5–8] Frankel and Weihs,[5,6] applying their work to shaped charges, derived a time-dependent exact solution for the free surface motion of a Newtonian jet and examined the linear stability of this solution within the Navier–Stokes equations. The extensional motion of the unperturbed flow follows from the observation that the jet produced by a shaped charge increases linearly in the axial direction. Henderson *et al.*,[7] applying their work to droplet formation, extended Frankel and Weihs' exact solution by including gravitational effects and conducted a related stability analysis. When a drop falls from its source it draws out a filament that connects the drop to its source,[7,9–15] as shown in Fig. 1; the solution considered by Henderson *et al.* applies during the transient period when this filament is cylindrical[7,9,13] [between (d) and (f) in Fig. 1]. In experiments, the prediction for the time-dependent thinning of a Newtonian filament was verified by Henderson *et al.* and the stability results correctly predicted features of the filament's breakup for several viscous fluids.[7] Smolka *et al.*[8] generalized the exact solution for a Newtonian filament[7] to a viscoelastic filament using the Oldroyd-B constitutive model. Their prediction for the time-dependent thinning of a viscoelastic filament was verified in experiments for several semidilute polymer solutions.[8] Other studies have examined the extensional motion of falling drops in the low Reynolds number limit.[17,18]

Free surface extensional flows also appear in extensional rheometry devices. Matta and Tytus[1] developed a novel approach for measuring extensional viscosity by placing a fixed volume of liquid between two circular plates and allowing the bottom plate to fall from rest as the upper plate was held stationary. This constant force experiment creates a thinning filament, or liquid bridge, drawn out between the plates whose extensional viscosity and stretch rate are time dependent. The filament stretching rheometer,[2,3] which is a modification of Matta and Tytus' experiment, allows the separation rate of the plates to be controlled; in particular, steady extensional viscosity is obtained by displacing the plates exponentially in time. Under these conditions, along the midsection of the filament the stretch rate $\dot{\varepsilon}_0$ is constant (a desirable feature for measuring extensional viscosity), and the axial stress increases while the diameter decreases exponentially in time. In a recent analytical study, Matallah *et al.*[4] compared the effects of separating the filament stretching rheometer plates linearly versus exponentially in time for an Oldroyd-B fluid. They found in the linear case that after a transient period, the stretch rate and axial stress decrease in time allowing longer filament lengths and stretch times to be achieved compared to the exponential case. Although the studies by Frankel and Weihs,[5,6] Henderson *et al.*,[7] Smolka *et al.*,[8] and Matallah *et al.*[4] are applied to different physical

a)Electronic mail: lsmolka@bucknell.edu.
b)Electronic mail: witelski@math.duke.edu.

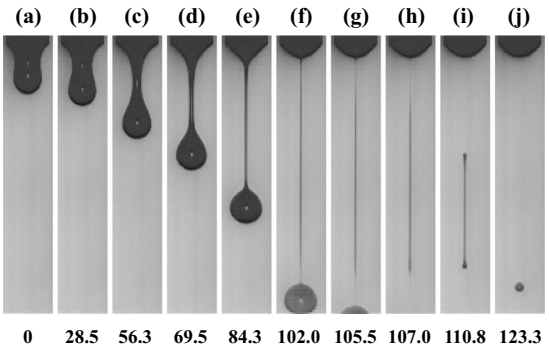

FIG. 1. The formation and breakup of a filament drawn out by a drop that is falling due to gravity. The filament is cylindrical during a transient period between frames (d) and (f) (Refs. 7 and 16). The relative time in ms is provided below each image and the length of each image is 2.57 cm. The kinematic viscosity, surface tension, and density of the fluid are 1.06 cm^2/s, 21.5 dyn/cm, and 0.928 g/cm^3, respectively. The mean flow rate at the nozzle is 6.8×10^{-3} cm^2/s and the Reynolds and Weber numbers of the flow are $O(1)$ and $O(10^{-7})$, respectively.

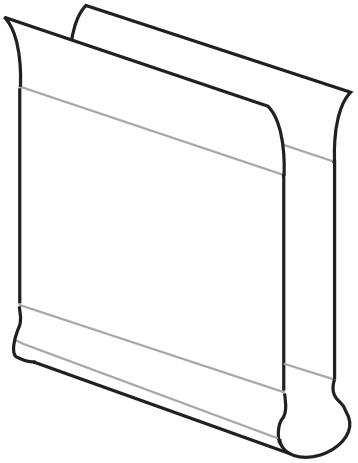

FIG. 2. A snapshot in time of an idealized planar sheet drawn out by a nearly constant volume of fluid falling from a rectangular orifice. The sheet is the analog of a cylindrical filament that forms behind a falling drop as shown in Fig. 1.

systems, they describe the same kinematic flow in which the time dependence of the stretch rate $[\dot{\varepsilon}(t)\sim 1/t]$ and that of the filament length $[L(t)\sim t]$ balance so as to conserve filament volume. In all of these studies, the flow is inertially driven. The kinematics of an extensional flow can be quite different when the flow is not inertially driven.[1,17,18] In particular, in the filament rheometer experiments by Matta and Tytus,[1] $\dot{\varepsilon}\sim 1/t$ and $L(t)\sim t^2$ as a result of the flow starting from rest, while in the low Reynolds number studies of falling drops,[17,18] $\dot{\varepsilon}\sim$ const and $L(t)\sim e^t$.

Here we extend the work of Henderson *et al.*[7] for a uniaxial extensional flow to the case of an idealized planar extensional flow. In particular, we derive an exact solution for an inertially driven base flow with a planar free surface using the full Navier–Stokes equations. The resulting stretch rate of the flow will be shown to be inversely dependent on time. Given the analogous nature of our work to Ref. 7, we imagine that the idealized flow considered here could be applied to a planar sheet drawn out by a nearly constant volume of fluid falling from a rectangular orifice (Fig. 2). In particular, at low mean flow rate, the fluid mass at the rectangular orifice will attain various equilibrium shapes until surface tension can no longer support its weight and the mass begins to fall. The formation of the planar sheet should occur over a transient period as the fluid mass elongates; Fig. 2 illustrates an instant in time during the sheet's evolution. These dynamics are similar to the way in which a falling drop of nearly constant volume draws out a cylindrical filament (Fig. 1).[7,9–15] There is, of course, an important difference between planar and cylindrical flows. In the cylindrical case, surface tension through the hoop curvature is always present and destabilizes the flow (referred to as the capillary instability[19]), whereas in the planar case this effect is absent. For this reason, we expect the stabilities of cylindrical and planar extensional flows to be quite different. The dynamics of the free end of the sheet, after the sheet becomes unstable, can be described by Taylor's model for the retraction and disintegration of sheets,[20] just as the dynamics of a free filament after drop pinch-off [Figs. 1(h) and 1(i)] is analyzed by Clanet and Lasheras;[21] our study will not focus on these later time dynamics.

The planar flows found in curtain coating, film casting, and spray atomization have received considerable attention in theoretical and experimental studies seeking to understand their motion[22–24] and stability.[25–38] These flows are, however, quite different than the planar extensional flow we consider here in several ways, notably in the following:

(1) Curtain coating, film casting, and spray atomization flows are steady, whereas the planar extensional sheet flow we consider is time-dependent.
(2) The thickness of a curtain coating flow is tapered in the axial direction, whereas the profile of our planar extensional sheet is spatially uniform.
(3) The axial velocity of curtain coating and film casting flows increases nonlinearly in the axial direction following a prediction made by Taylor,[22] whereas the axial velocity of our planar extensional flow increases linearly in the axial direction.
(4) The reciprocal of the stretch rate sets a time scale in a planar extensional flow;[4] curtain coating, film casting, and spray atomization flows are not extensional flows and therefore do not share this time scale.

These differences make it difficult to directly compare the stability of curtain coating, film casting, and spray atomization flows to the planar extensional flow we consider here. Other studies motivated by manufacturing processes of polymer melts (e.g., film blowing) have examined the stability of planar sheets and films either in steady multiaxial extension or nearly multiaxial extensional flows.[39,40] Romero[41] extended Frankel and Weihs' time-dependent solution to plastic sheets subject to time-dependent biaxial extensional flow with acceleration acting in the normal direction; he studied linear stability using a primarily numerical approach. We will use asymptotics to analyze the transient and long-time behaviors for the linear stability of a Newtonian sheet with acceleration acting in the axial direction.

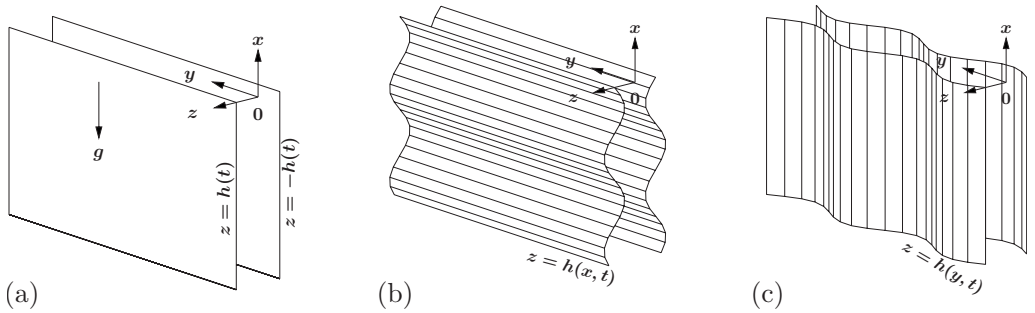

FIG. 3. Schematic of a liquid sheet with free surfaces located at $z=\pm h$: (a) unperturbed $z=\pm h(t)$; (b) symmetric perturbations in the axial direction, $z=\pm h(x,t)$; and (c) symmetric perturbations in the transverse direction, $z=\pm h(y,t)$.

The perturbed motion of a planar sheet can be decomposed into symmetric and antisymmetric motions (also called varicose and sinuous motions, respectively) as described by Taylor.[42] Varicose motions are symmetric about the planar axis, whereas sinuous motions conserve the sheet thickness while allowing variations in the sheet midplane. In this work, we analyze the temporal linear stability of our exact solution for a planar extensional sheet to symmetric perturbations imposed in the axial and transverse directions [see Figs. 3(b) and 3(c)] while neglecting the influence of any surrounding gas. Owing to the time dependence of the exact solution, the stability analysis involves solving an initial value problem rather than a normal-mode eigenvalue problem.[5–7] Utilizing the fact that our exact solution derived from the full Navier–Stokes equations also satisfies the long-wave model for a liquid sheet, we examine the sheet's stability within the framework of the simpler long-wave model for both inviscid and viscous fluids. We will show that transient growth and asymptotic stability of perturbations are important in understanding the dynamics of planar extensional sheets.

The paper is organized as follows. In Sec. II, the governing equations to the free boundary problem are described and an exact solution for the unperturbed flow of a Newtonian sheet is derived. In Sec. III, we show that this exact solution satisfies the long-wave model for a thin liquid sheet and examine the stability of inviscid and viscous sheets in the long-wave limit in Secs. V–VII. Conclusions are provided in Sec. VIII.

II. FREE BOUNDARY PROBLEM AND AN EXACT SOLUTION

Here we formulate the free boundary problem for the planar extensional motion of an inertially driven fluid sheet. We will show that a closed-form time-dependent solution exists given an appropriate initial state for the sheet. The initial conditions can be generated by the action of dominant forces in earlier stages of the dynamics, analogous to the case of uniaxial extensional flows (e.g., a first-stage explosive device for a shaped charge and gravity for the dripping drop).

Consider the motion of an incompressible viscous fluid governed by the Navier–Stokes equations

$$\rho[\partial_t \mathbf{u} + (\mathbf{u}\cdot\nabla)\mathbf{u}] = -\nabla p + \mu\nabla^2\mathbf{u} - \rho\mathbf{g}, \tag{1a}$$

$$\nabla\cdot\mathbf{u} = 0, \tag{1b}$$

where ρ is the density, $\mathbf{u}=(u,v,w)$ is the velocity field with u, v, and w being the axial, transverse, and in-plane velocity components, p is the pressure, μ is the dynamic viscosity, and $\mathbf{g}=g\hat{\mathbf{e}}_\mathbf{x}$ is gravity with $\hat{\mathbf{e}}_\mathbf{x}$ directed upward. It will be seen that gravity is not the primary driving force in this problem, but if present, it must act in the direction that the flow is stretching, i.e., the axial direction.

We examine symmetric motions of a planar liquid sheet whose boundaries are free surfaces, denoted by $z=\pm h(x,y,t)$, with examples shown in Fig. 3. At the free surfaces, $z=\pm h$, there are three boundary conditions:

(i) the kinematic condition,

$$\partial_t h + u\partial_x h + v\partial_y h = w, \tag{2a}$$

(ii) the normal stress condition,

$$\mathbf{n}\cdot(\mathbf{T}-p\mathbf{I})\cdot\mathbf{n} = -\gamma\nabla\cdot\mathbf{n}, \tag{2b}$$

where $\mathbf{n}=\pm(-\partial_x h,-\partial_y h,1)/\sqrt{(\partial_x h)^2+(\partial_y h)^2+1}$ is the outward unit normal vector to the free surface at $z=\pm h$, $\mathbf{T}=\mu(\nabla\mathbf{u}+\nabla\mathbf{u}^T)$ is the extra stress field for a Newtonian fluid, $\mathbf{I}$ is the identity tensor, and γ is the coefficient of surface tension, and

(iii) the tangential stress condition,

$$\mathbf{n}\cdot(\mathbf{T}-p\mathbf{I})\cdot\mathbf{t}_1 = 0, \tag{2c}$$

$$\mathbf{n}\cdot(\mathbf{T}-p\mathbf{I})\cdot\mathbf{t}_2 = 0, \tag{2d}$$

corresponding to the tangent vectors to the free surface $\mathbf{t}_1=(1,0,\partial_x h)$ and $\mathbf{t}_2=(0,1,\partial_y h)$. For symmetric motions of the liquid sheet[23] we require

$$w=0, \quad \partial_z p=0, \quad \partial_z u=0 \quad \text{at } z=0. \tag{3}$$

Equations (1a), (1b), (2a)–(2d), and (3) define the free boundary problem for the motion of a Newtonian sheet that is infinite in extent. Since only symmetric motions of the sheet will be considered here, the flow may be analyzed from $z=0$ to $z=h$ without loss of generality.

For the unperturbed flow we shall assume that the sheet is spatially uniform, consistent with previous studies on cylindrical liquid filaments,[5–8]

$$\partial_x h = \partial_y h = 0, \tag{4}$$

as shown in Fig. 3(a). We consider a velocity field with the form

$$\mathbf{u} = (u,v,w) = [\dot{\varepsilon}(t)x + \eta(t), 0, -\dot{\varepsilon}(t)z], \tag{5}$$

which is a combination of a planar extensional flow $[\dot{\varepsilon}(t)x, 0, -\dot{\varepsilon}(t)z]$ where $\dot{\varepsilon}(t)$ represents the stretch rate,[39,43] and a spatially uniform flow $[\eta(t), 0, 0]$ which is required to balance gravitational effects[7] as we will show next. For a spatially uniform sheet, the velocity field [Eq. (5)] conserves mass [Eq. (1b)] and satisfies the boundary conditions at the free surface [Eqs. (2a), (2c), and (2d)] and midplane [Eq. (3)]. The x axis is the distinguished direction in which we assume extension will take place; in the y direction there is no flow. The extra stress field associated with this velocity field is diagonal with components

$$T_{xx} = 2\mu\dot{\varepsilon}(t), \quad T_{yy} = 0, \quad T_{zz} = -2\mu\dot{\varepsilon}(t). \tag{6}$$

Using the planar extensional velocity field [Eq. (5)], the free boundary problem for the unperturbed flow is described by the Navier–Stokes equations (1a) in the x, y, and z directions

$$\frac{\partial p}{\partial x} = -\rho\left(\frac{d\dot{\varepsilon}}{dt} + \dot{\varepsilon}^2\right)x - \rho\left(\frac{d\eta}{dt} + \dot{\varepsilon}\eta + g\right), \tag{7a}$$

$$\frac{\partial p}{\partial y} = 0, \tag{7b}$$

$$\frac{\partial p}{\partial z} = \rho\left(\frac{d\dot{\varepsilon}}{dt} - \dot{\varepsilon}^2\right)z, \tag{7c}$$

and the kinematic [Eq. (2a)] and normal [Eq. (2b)] boundary conditions evaluated at $z=h(t)$ become

$$\frac{dh}{dt} = -\dot{\varepsilon}h, \tag{7d}$$

$$p(x,y,h,t) = -2\mu\dot{\varepsilon} + p_{\text{amb}}, \tag{7e}$$

where we have used the fact that an unperturbed sheet is spatially uniform $[h=h(t)]$ and p_{amb} is the ambient pressure. The tangential boundary conditions (2c) and (2d) are identically satisfied by the planar extensional velocity field [Eq. (5)]. From Eq. (7b) we conclude that $p=p(x,z,t)$.

Taking the derivative of Eq. (7e) with respect to x yields

$$\partial_x p = 0 \quad \text{at } z = h(t). \tag{8}$$

Substituting this into Eq. (7a) then collecting powers of x results in two first-order ordinary differential equations (ODEs),

$$\frac{d\dot{\varepsilon}}{dt} + \dot{\varepsilon}^2 = 0, \tag{9a}$$

$$\frac{d\eta}{dt} + \dot{\varepsilon}\eta + g = 0, \tag{9b}$$

which can be solved exactly. In Eq. (9b) we see the need for the extra axial velocity component $\eta(t)$ to balance the gravitational term; in the absence of η, the velocity field [Eq. (5)] is inconsistent. The solutions of Eq. (9) are

$$\dot{\varepsilon}(t) = \frac{1}{t+t_0} \quad \text{and} \quad \eta(t) = -\frac{g}{2}(t+t_0) - \frac{\check{x}}{t+t_0}, \tag{10}$$

where $\dot{\varepsilon}_0$ is the initial stretch rate, $t_0 = 1/\dot{\varepsilon}_0 > 0$ is consistent with stretching in x for all later times, and $\check{x}$ is a fixed axial position in the laboratory reference frame. It follows that the corresponding velocity components [Eq. (5)] are

$$u(x,t) = \frac{x-\check{x}}{t+t_0} - \frac{g}{2}(t+t_0), \quad v = 0, \quad w(z,t) = -\frac{z}{t+t_0}. \tag{11a}$$

The position $\check{x}$ can be interpreted in terms of the initial conditions as follows: if at $t=0$ x' is the axial position where the axial velocity vanishes, then $\check{x}$ can be obtained in terms of x' from Eq. (11a),

$$u(x',0) = 0 \quad \rightarrow \quad \check{x} = x' - \tfrac{1}{2}gt_0^2;$$

in the absence of gravity $\check{x}=x'$. Using the kinematic condition (7d), the free surface is described by

$$h(t) = \frac{\mathbb{H}t_0}{t+t_0}, \tag{11b}$$

where $h(0)=\mathbb{H}>0$ is the initial half-thickness of the sheet. Integrating Eq. (7c) in z and then using the normal stress condition Eq. (7e) yields the pressure field

$$p(z,t) = \rho\frac{h^2 - z^2}{(t+t_0)^2} - \frac{2\mu}{t+t_0} + p_{\text{amb}}, \tag{11c}$$

which is independent of x and the surface tension γ, as one would expect for a planar sheet.

Equations (11a)–(11c) describe an exact solution to the free boundary problem of an infinite planar sheet of Newtonian fluid stretching as a planar extensional flow. This solution is valid for any value for the viscosity $(\mu \geq 0)$ and is independent of surface tension. The solution is also well defined for all values of axial acceleration g. If gravity is present, then the sheet will be subject to constant acceleration while it stretches. To see this, we construct a Lagrangian description of the flow, denoting the position of a fluid particle in the sheet by $[x(t), y(t), z(t)]$. The motion of a typical fluid particle, starting from position (x_0, y_0, z_0) at $t=0$, is found by solving $d\mathbf{x}/dt = \mathbf{u}$,

$$\frac{dx}{dt} = \frac{x-\check{x}}{t+t_0} - \frac{g}{2}(t+t_0), \quad \frac{dy}{dt} = 0, \quad \frac{dz}{dt} = -\frac{z}{t+t_0}. \tag{12}$$

The result is

$$x(t;x_0) = -\frac{1}{2}g(t+t_0)^2 + \left(\frac{x_0 - \check{x} + \frac{1}{2}gt_0^2}{t_0}\right)(t+t_0) + \check{x}, \tag{13a}$$

$$y(t;y_0) = y_0, \tag{13b}$$

$$z(t;z_0) = \frac{z_0 t_0}{t + t_0}, \tag{13c}$$

where $|z_0| \leq \mathbb{H}$. Interpreting these results, we find from Eq. (13a) that each fluid particle is falling in a uniform gravitational field and from Eq. (13b) that there is no flow in the transverse direction. Equation (13c) also has a simple interpretation. Since the velocity gradient in the axial direction $[\partial u/\partial x = 1/(t+t_0)$ following Eq. (11a)] is positive and independent of x, the sheet is stretching homogeneously in the vertical direction. In order to conserve mass, the stretching of the sheet must be balanced by contraction in the thickness, which accounts for the time dependence of the free surface in Eqs. (11b) and (13c); i.e., consider a volume element, $\Delta V = \Delta x \Delta y \Delta z$, we see from Eq. (13) that the $O(1/t)$ thinning in the z direction is balanced by linear stretching in the x direction.

It is worth noting that inertia drives the unperturbed flow by setting the time dependence of the stretch rate $\dot{\varepsilon}$; this is evident from the ODE for $\dot{\varepsilon}$ [Eq. (9a)] which contains only inertial terms from the axial momentum equation (7a). Given the coupling of the free surface (h) to the stretch rate in Eq. (7d), we find that inertia also sets the time scale of h where both the stretch rate and free surface are monotonically decreasing functions of time. Given the coupling of the velocity field to the stretch rate and $\eta(t)$ [Eq. (5)], we find that the velocity is driven by inertial and gravitational effects.

The planar extensional flow [Eq. (11)] is the analog of a uniaxial extensional flow studied by Henderson *et al.*[7] who applied their work to the free surface motion of a spatially uniform filament drawn out by a viscous drop dripping from its source (see Fig. 1). We propose an analogous experiment in which a planar sheet of fluid is drawn out by a constant volume of fluid dripping from a rectangular orifice (see Fig. 2) with the experimental control parameters given by the initial stretch rate and sheet thickness (which can be set by adjusting the width of the rectangular orifice). We recognize that maintaining the base flow [Eq. (11)] will be difficult with a Newtonian fluid for two reasons. First, our stability analysis suggests that inviscid and viscous sheets are unstable to transverse perturbations. Second, the experiment would be limited to a finite-size sheet where the behavior of the flow could be quickly overwhelmed by edge effects. The base flow could be more experimentally feasible with strain-hardening materials (e.g., viscoelastic fluids and polymer melts) that display high Trouton ratios in extensional flows.[2,3] This stabilizing mechanism could dampen the edge effects expected in a finite-sized sheet. Nevertheless, this is the first study that we are aware of that examines inertially driven planar extensional sheets, and the Newtonian analysis is the logical first step to analyzing this flow.

Next, we show that the exact solution to the Navier–Stokes equations (11) also satisfies the long-wave model for a thin liquid sheet. Using this fact, we investigate the stability of the exact solution in the long-wave limit.

III. LONG-WAVE MODEL

Equation (11) describes an exact solution of the full equations of free surface flow for a Newtonian sheet; no approximations or simplifications have been made to the governing equations so far. The long-wave model or slender body equations are derived based on the assumption that the sheet is very thin compared to the length scale of variations along the sheet. Solution (11) clearly fits this framework as the sheet is uniform in space and it becomes progressively thinner as time increases [Eq. (11b)]. So, we will make use of the long-wave model as a simpler framework to work within for analytically studying the stability of the sheet solution to symmetric perturbations.

We begin by nondimensionalizing the governing equations (1a), (1b), (2a)–(2d), (3), and (6) with respect to a characteristic axial length scale $\mathbb{L}$, the initial sheet half-thickness $\mathbb{H}$, and a typical axial velocity $\mathbb{U}$,

$$x = \mathbb{L}\hat{x}, \quad y = \mathbb{L}\hat{y}, \quad z = \mathbb{H}\hat{z}, \quad h = \mathbb{H}\hat{h},$$

$$u = \mathbb{U}\hat{u}, \quad v = \mathbb{U}\hat{v}, \quad w = \frac{\mathbb{H}\mathbb{U}}{\mathbb{L}}\hat{w}, \quad t = \frac{\mathbb{L}}{\mathbb{U}}\hat{t}, \quad p = \frac{\mu \mathbb{U}}{\mathbb{L}}\hat{p},$$

where the hat notation refers to dimensionless quantities. Using these scaled variables the governing equations (1a), (1b), (2a)–(2d), (3), and (6) will depend on a few key dimensionless parameters,

$$\mathrm{Re} = \frac{\rho \mathbb{U}\mathbb{L}}{\mu}, \quad \mathrm{We} = \frac{\rho \mathbb{U}^2 \mathbb{L}^2}{\mathbb{H}\gamma}, \quad \mathrm{Fr} = \frac{\mathbb{U}}{\sqrt{g\mathbb{L}}}. \tag{14}$$

These are the Reynolds number, which compares inertial to viscous effects, the Weber number, which compares inertial to surface tension effects, and the Froude number. The principal time scale in the problem is the reciprocal of the initial stretch rate $t_0 = 1/\dot{\varepsilon}_0$, which we use to define the velocity scale, namely, $\mathbb{U} = \mathbb{L}\dot{\varepsilon}_0$.

Long-wave asymptotics in the limit of small aspect ratio, $\mathbb{H}/\mathbb{L} \to 0$, can be used to reduce the governing equations to a leading order system for the thickness of the sheet, $h(x,y,t)$, and the in-plane, thickness-averaged velocity, $\mathbf{u} \equiv [u(x,y,t), v(x,y,t)]$ (dropping the hats for convenience),

$$\partial_t h + \nabla \cdot (h\mathbf{u}) = 0, \tag{15a}$$

$$\partial_t \mathbf{u} + \mathbf{u} \cdot \nabla \mathbf{u} = \frac{1}{h\,\mathrm{Re}} \nabla \cdot (h[\nabla \mathbf{u} + \nabla \mathbf{u}^{\mathbf{T}} + 2(\nabla \cdot \mathbf{u})\mathbf{I}]) + \frac{1}{\mathrm{We}} \nabla (\nabla^2 h) - \frac{1}{\mathrm{Fr}^2}\hat{\mathbf{e}}_x, \tag{15b}$$

see Ref. 44 for a detailed derivation. A similar derivation is used to develop simplified equations for a thin, axisymmetric, fluid cylinder.[45] For solutions independent of y and with $v = 0$ (i.e., $h = h(x,t), \mathbf{u} = [u(x,t), 0]$), these equations reduce to the more familiar one-dimensional (1D) equations for conservation of mass and momentum in the axial direction,[46,47]

$$\partial_t h + \partial_x (hu) = 0, \tag{16a}$$

$$\partial_t u + u\partial_x u = \frac{4}{h\,\mathrm{Re}}\partial_x(h\partial_x u) + \frac{1}{\mathrm{We}}\partial_{xxx}h - \frac{1}{\mathrm{Fr}^2}. \tag{16b}$$

Comparable equations for extensional flow of axisymmetric jets with surface tension, inertia, and gravity were obtained in Ref. 48.

The nondimensional form of the exact solution for u [Eq. (11a)] and h [Eq. (11b)] derived from the full Navier–Stokes equations, which we now refer to as u_0 and h_0, are

$$h_0(t) = \frac{1}{t+1}, \quad u_0(x,t) = \frac{x-\check{x}}{t+1} - \frac{t+1}{2\,\mathrm{Fr}^2}. \tag{17}$$

One can easily verify that the exact solution (17) also satisfies the long-wave model [Eqs. (15) and (16)]. Next, working within the framework of this long-wave model, we analyze the linear stability of the exact time-dependent solution.

IV. FORMULATION OF THE LINEAR STABILITY PROBLEM

We consider the linear stability of the exact solution (17) within the simpler framework of the long-wave model [Eq. (15)] rather than the full Navier–Stokes equations. Using a temporal analysis we consider the stability of inviscid and viscous planar sheets to symmetric perturbations acting in the axial (x) and transverse (y) directions. Perturbing around the solution in Eq. (17),

$$h(x,y,t) = h_0(t) + \delta h_1(x,y,t), \tag{18a}$$

$$u(x,y,t) = u_0(x,t) + \delta u_1(x,y,t), \tag{18b}$$

$$v(x,y,t) = 0 + \delta v_1(x,y,t), \tag{18c}$$

with $\delta \ll 1$; then substituting into Eq. (15) and keeping only linear terms in the perturbed variables results in a set of linearized equations in terms of h_1, u_1, and v_1,

$$\partial_t h_1 + \left(\frac{x-\check{x}}{t+1} - \frac{t+1}{2\,\mathrm{Fr}^2}\right)\partial_x h_1 + \frac{h_1}{t+1} + \frac{1}{t+1}\partial_x u_1 + \frac{1}{t+1}\partial_y v_1 = 0, \tag{19a}$$

$$\partial_t u_1 + \left(\frac{x-\check{x}}{t+1} - \frac{t+1}{2\,\mathrm{Fr}^2}\right)\partial_x u_1 + \frac{u_1}{t+1} = \frac{1}{\mathrm{Re}}(4\partial_x h_1 + 4\partial_{xx}u_1 + 3\partial_{xy}v_1 + \partial_{yy}u_1) + \frac{1}{\mathrm{We}}(\partial_{xxx}h_1 + \partial_{xyy}h_1), \tag{19b}$$

$$\partial_t v_1 + \left(\frac{x-\check{x}}{t+1} - \frac{t+1}{2\,\mathrm{Fr}^2}\right)\partial_x v_1 = \frac{1}{\mathrm{Re}}(2\partial_y h_1 + \partial_{xx}v_1 + 3\partial_{xy}u_1 + 4\partial_{yy}v_1) + \frac{1}{\mathrm{We}}(\partial_{yyy}h_1 + \partial_{xxy}h_1). \tag{19c}$$

For convenience we change variables to characteristic coordinates suggested by the left-hand sides of Eq. (19). Let $(x,t) \to (\chi,\tau)$ with

$$\chi = \frac{x-\check{x}}{\tau} + \frac{\tau}{2\,\mathrm{Fr}^2}, \quad \tau = t+1, \tag{20}$$

so that

$$\partial_x = \frac{1}{\tau}\partial_\chi, \quad \partial_t = \partial_\tau - \left(\frac{x-\check{x}}{\tau^2} - \frac{1}{2\,\mathrm{Fr}^2}\right)\partial_\chi. \tag{21}$$

In particular, the convective derivative $\partial_t + u_0\partial_x \to \partial_\tau$. In these variables the exact solution takes the form $h_0 = 1/\tau$ and $u_0 = \chi - \tau/\mathrm{Fr}^2$. Then Eq. (19) can be simplified to

$$\partial_\tau h_1 + \frac{h_1}{\tau} + \frac{1}{\tau^2}\partial_\chi u_1 + \frac{1}{\tau}\partial_y v_1 = 0, \tag{22a}$$

$$\partial_\tau u_1 + \frac{u_1}{\tau} = \frac{1}{\mathrm{Re}}\left(\frac{4}{\tau}\partial_\chi h_1 + \frac{4}{\tau^2}\partial_{\chi\chi}u_1 + \frac{3}{\tau}\partial_{\chi y}v_1 + \partial_{yy}u_1\right) + \frac{1}{\mathrm{We}}\left(\frac{1}{\tau^3}\partial_{\chi\chi\chi}h_1 + \frac{1}{\tau}\partial_{\chi yy}h_1\right), \tag{22b}$$

$$\partial_\tau v_1 = \frac{1}{\mathrm{Re}}\left(2\partial_y h_1 + \frac{1}{\tau^2}\partial_{\chi\chi}v_1 + \frac{3}{\tau}\partial_{\chi y}u_1 + 4\partial_{yy}v_1\right) + \frac{1}{\mathrm{We}}\left(\partial_{yyy}h_1 + \frac{1}{\tau^2}\partial_{\chi\chi y}h_1\right). \tag{22c}$$

Note that this system is independent of the Froude number.

We look for solutions h_1, u_1, and v_1 in the form of Fourier transform integrals

$$h_1(\chi,y,\tau) = \int_{-\infty}^{\infty}\int_{-\infty}^{\infty} H_1(k_\chi,k_y,\tau)e^{i(k_\chi\chi + k_y y)}dk_\chi dk_y, \tag{23a}$$

$$u_1(\chi,y,\tau) = \int_{-\infty}^{\infty}\int_{-\infty}^{\infty} U_1(k_\chi,k_y,\tau)e^{i(k_\chi\chi + k_y y)}dk_\chi dk_y, \tag{23b}$$

$$v_1(\chi,y,\tau) = \int_{-\infty}^{\infty}\int_{-\infty}^{\infty} V_1(k_\chi,k_y,\tau)e^{i(k_\chi\chi + k_y y)}dk_\chi dk_y, \tag{23c}$$

where the wavenumbers k_χ, k_y are real. Noting that the system (22a)–(22c) has terms with coefficients that depend only on τ (and not χ and y), then substituting Eq. (23) into Eq. (22) reduces the coupled system of partial differential equations for h_1, u_1, v_1 to a coupled system of ODEs for the Fourier coefficients H_1, U_1, V_1,

$$\frac{dH_1}{d\tau} = -\frac{H_1}{\tau} - \frac{ik_\chi}{\tau^2}U_1 - \frac{ik_y}{\tau}V_1, \tag{24a}$$

$$\frac{dU_1}{d\tau} = -\frac{U_1}{\tau} - \frac{1}{\mathrm{Re}}\left(-\frac{4ik_\chi}{\tau}H_1 + \frac{4k_\chi^2}{\tau^2}U_1 + \frac{3k_\chi k_y}{\tau}V_1 + k_y^2 U_1\right) - \frac{i}{\mathrm{We}}\left(\frac{k_\chi^3}{\tau^3} + \frac{k_\chi k_y^2}{\tau}\right)H_1, \tag{24b}$$

$$\frac{dV_1}{d\tau} = -\frac{1}{\mathrm{Re}}\left(-2ik_yH_1 + \frac{k_\chi^2}{\tau^2}V_1 + \frac{3k_\chi k_y}{\tau}U_1 + 4k_y^2V_1\right) - \frac{i}{\mathrm{We}}\left(\frac{k_\chi^2 k_y}{\tau^2} + k_y^3\right)H_1. \tag{24c}$$

We make a few comments before proceeding:

(1) Standard temporal normal-mode stability analyses about a steady base solution involve perturbations that are exponentials in time; stability is defined in terms of a dispersion relation that relates the exponential growth rate to the perturbation wavenumber. The temporal stability analysis presented here is different in two ways. First, the base solution is spatially and temporally dependent [Eq. (17)]. Second, we do not *a priori* assume the form of the temporal dependence of the perturbations [Eq. (23)]. In this analysis, stability depends on the temporal growth of the perturbed variables relative to the base solution, in particular, we classify the solution as stable if v_1 is *a priori* bounded and $h_0 \gg h_1$ and $u_0 \gg u_1$ for all time. The connection between the temporal dependence of the perturbed variables and wavenumber (k_χ, k_y) will be made explicit in our analysis. Our main focus will be on the behavior of h_1 in the presentation that follows.

(2) The characteristic axial coordinate χ [Eq. (20)] corresponds to the Lagrangian description [Eq. (13a)] for the unperturbed flow. The extensional stretching of the sheet in the axial direction gets mapped onto a fixed interval in terms of χ. In writing Eq. (23), we assume that spatial perturbations will follow the same stretching; this approach has been used in Refs. 5–7. Converting to the Eulerian frame, assuming k_χ is constant implies that the perturbation wavelength will be observed to increase linearly with time, $\lambda = 2\pi/k_x$ with $k_x = k_\chi/\tau$.

(3) The system (24a)–(24c) can be written in vector form as

$$\mathbf{X} = \begin{pmatrix} H_1 \\ U_1 \\ V_1 \end{pmatrix}, \quad \frac{d\mathbf{X}}{d\tau} = \mathbf{M}(\tau)\mathbf{X}. \tag{25}$$

For all finite τ, this is a nonautonomous non-normal system, i.e., $\mathbf{MM^T} \neq \mathbf{M^TM}$, and hence the stability analysis can be expected to be nontrivial.[49–51]

(4) Although the Fourier coefficients H_1, U_1, V_1 are functions of k_χ, k_y, τ we will suppress the dependence on the k_χ, k_y parameters for notational convenience hereafter.

(5) In terms of τ, the initial time is $\tau = 1$, see Eq. (20).

To quantify the influence of perturbations imposed in the axial and transverse directions, we first present the 1D analysis with perturbations imposed in only k_χ or k_y, before discussing the full two-dimensional (2D) analysis.

V. 1D PERTURBATIONS IN THE AXIAL DIRECTION

We begin by considering perturbations that are solely in the axial direction, that is, they are independent of the transverse direction and have $k_y = 0$. With $k_y = 0$, the Eqs. (24a)–(24c) reduce to

$$\frac{dH_1}{d\tau} = -\frac{H_1}{\tau} - \frac{ik_\chi}{\tau^2}U_1, \tag{26a}$$

$$\frac{dU_1}{d\tau} = -\frac{U_1}{\tau} - \frac{4}{\mathrm{Re}}\left(-\frac{ik_\chi}{\tau}H_1 + \frac{k_\chi^2}{\tau^2}U_1\right) - \frac{ik_\chi^3}{\tau^3\,\mathrm{We}}H_1, \tag{26b}$$

$$\frac{dV_1}{d\tau} = -\frac{k_\chi^2}{\tau^2\,\mathrm{Re}}V_1. \tag{26c}$$

Observe that Eq. (26c) decouples from the rest of Eq. (26). For initial condition $V_1(1) = V^0$, the explicit solution of Eq. (26c) is

$$V_1(\tau) = V^0 e^{k_\chi^2\,\mathrm{Re}^{-1}(\tau^{-1}-1)} \tag{27}$$

and $|V_1(\tau)| < |V^0|$ for all $\tau > 1$; therefore infinitesimal perturbations to v remain bounded by the initial disturbance amplitude for all times. Hence the flow is linearly stable with respect to such perturbations in this velocity component.

We will show that in all cases (short/long waves and viscous/inviscid), the long-time asymptotics of perturbations to the sheet thickness are the same,

$$H_1(\tau) \sim \frac{\alpha}{\tau} + o(\tau^{-1}) \quad \text{as} \quad \tau \to \infty. \tag{28}$$

Relative to the base solution $h_0(\tau)$, one could naively believe that Eq. (28) implies that all 1D perturbations in the axial direction have marginal asymptotic stability. That is, the ratio $|H_1/h_0|$ is bounded as $\tau \to \infty$, but as we will show, the coefficient α can become large as a result of *transient growth of the perturbations*[51–56] and more careful consideration of the stability is needed.

To quantify this behavior we define an asymptotic amplification factor α as the maximal value (over all choices of initial conditions) of the absolute ratio,

$$\alpha \equiv \lim_{\tau\to\infty}\left|\frac{H_1(\tau)/h_0(\tau)}{H_1(1)/h_0(1)}\right|. \tag{29}$$

This parameter is similar in form to the growth ratios defined in Ref. 57 and describes the ratio of the relative size of a perturbation for long times compared to its initial size. We normalize the perturbations so that H_1 starts with unit magnitude at $\tau = 1$,

$$|H_1(1)| = 1. \tag{30}$$

While in general $H_1(\tau)$ can be complex-valued, for convenience (and without significant loss of generality) we will pick initial conditions to make H_1 real and U_1 pure imaginary; the form of Eqs. (26a) and (26b) shows that these forms will be maintained for all time. This will be beneficial for distinguishing monotonic versus oscillatory behaviors.

We note that Eq. (29) simplifies to the limit of $|\tau H_1(\tau)|$, consistent with the form given in Eq. (28). This parameter determines if the long-time perturbations are indeed uniformly small starting from small initial conditions. As such α gives a measure of the sustained influence of the transient growth. This behavior has a nontrivial relationship to the initial conditions and transient time scales. In particular, the first time scale is set by the time when the initial conditions

are applied [Eq. (30)] and the other relevant times will become clear in our discussion of each of the following cases.

Focusing on the remaining system (26a) and (26b), to better understand the parameter dependence of the problem for $k_\chi \neq 0$ it is convenient to rescale these equations using

$$H_1(\tau) = H(T), \quad U_1(\tau) = \left(\frac{k_\chi}{\mathrm{We}}\right)^{1/3} U(T), \quad \tau = \left(\frac{k_\chi^4}{\mathrm{We}}\right)^{1/3} T, \tag{31}$$

yielding

$$\frac{dH}{dT} = -\frac{H}{T} - \frac{iU}{T^2}, \tag{32a}$$

$$\frac{dU}{dT} = -\frac{U}{T} - \omega\left(-\frac{iH}{T} + \frac{U}{T^2}\right) - \frac{iH}{T^3}, \tag{32b}$$

where the only remaining explicit parameter is

$$\omega = \frac{4}{\mathrm{Re}}[k_\chi^2\,\mathrm{We}]^{1/3}, \tag{33}$$

and the initial condition (30) becomes

$$H(T_0) = 1 \quad \text{at} \quad T_0 = \left(\frac{\mathrm{We}}{k_\chi^4}\right)^{1/3}. \tag{34}$$

System (32a) and (32b) can also be combined into a second-order ODE for $H(T)$,

$$\frac{d^2H}{dT^2} + \left(\frac{4}{T} + \frac{\omega}{T^2}\right)\frac{dH}{dT} + \left(\frac{2}{T^2} + \frac{1}{T^5}\right)H = 0, \tag{35}$$

where $U(T)$ can be obtained in terms of derivatives of the solution $H(T)$. This form is particularly convenient for some of our observations on properties of the perturbations of the sheet thickness.

A. Inviscid problem

The inviscid problem (Re=∞) is given by setting $\omega=0$ in Eq. (35). This reduced equation can be solved explicitly in terms of Bessel functions of order 1/3 to yield

$$H(T) = \left[a_1 J_{1/3}\left(\tfrac{2}{3}T^{-3/2}\right) + a_2 Y_{1/3}\left(\tfrac{2}{3}T^{-3/2}\right)\right]T^{-3/2}, \tag{36}$$

and similarly, $U(T)$ can also be written in terms of these Bessel functions. The constants of integration a_1, a_2 are determined by the initial values of the perturbations H, U. Making use of Eq. (36) we can obtain complete stability results explicitly for this case.

If T_0 is sufficiently large so that perturbations begin in the long-time regime, then applying the initial condition (34) to the asymptotic form of Eq. (36) valid for $T\to\infty$ yields

$$H(T) \sim \frac{b_1}{T}\left(1 - \frac{1}{6T^3}\right) + \frac{b_2}{T^2}\left(1 - \frac{1}{12T^3}\right) + O(T^{-7}), \tag{37}$$

where $b_1 \sim T_0$. Then Eq. (37) gives the approximate solution for $T_0 \le T < \infty$. Consequently, for $T\to\infty$ we have $H \sim T_0/T$ and Eq. (31) yields the bound

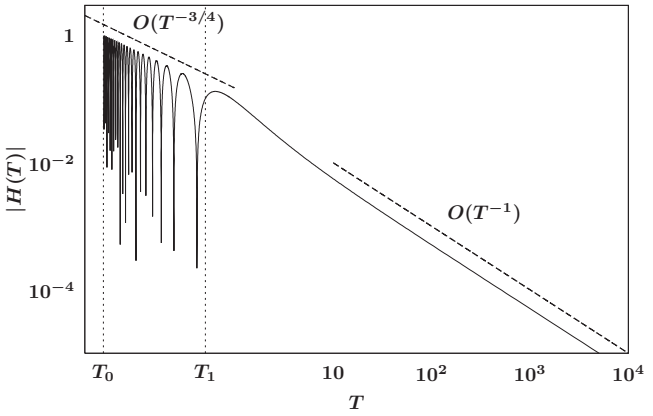

FIG. 4. Axial perturbations for inviscid sheets: Evolution of the perturbation amplitude in the short-wave case, $k_\chi > k_{\chi,1}$ or equivalently $T_0 < T_1$.

$$H_1(\tau) \le \frac{1}{\tau} \quad \text{as} \quad \tau\to\infty. \tag{38}$$

The definition of T_0 [Eq. (34)] shows that large T_0 corresponds to small wavenumbers k_χ. Hence $\alpha\to 1$ for $k_\chi\to 0$ and we conclude that long-wave perturbations are indeed marginally stable.

The case when T_0 is small is more interesting; applying the initial condition (34) to the asymptotic form of Eq. (36) valid for $T\to 0$ yields

$$H(T) \sim \frac{(T/T_0)^{-3/4}}{\cos\,\theta_0}\cos\left(\frac{2}{3}[T^{-3/2} - T_0^{-3/2}] + \theta_0\right), \tag{39}$$

where θ_0 is a phase constant related to the initial condition set on $U(T_0)$. The oscillatory nature of this solution is shown in Fig. 4. The period of the oscillations is nonuniform with the frequency diverging for $T\to 0$ and decreasing monotonically as time increases. Indeed $H(T)$ will have a "final" zero corresponding to the first zero of $a_1 J_{1/3}(S) + a_2 Y_{1/3}(S)$ where S is inversely related to T, $S = \frac{2}{3}T^{-3/2}$. Setting the argument of the cosine in Eq. (39) to $\pi/2$ yields an estimate for this last zero. Note that this value can be arbitrarily large for appropriate θ_0, however; then separation to the previous zero will also be very large. For the purpose of establishing a uniform criterion by which we can divide $H(T)$ into oscillatory versus long-time regimes [as represented by Eq. (37)], we note that the *next-to-the-last* zero of $H(T)$ can be bounded from above (independent of θ_0) in terms of the first positive zero of the Bessel function $Y_{1/3}(S_1)=0$ with $S_1 \approx 1.353$. This sets a time scale that defines the effective end of oscillatory dynamics,

$$T_1 \le \left(\tfrac{3}{2}S_1\right)^{-2/3} \approx 0.6238. \tag{40}$$

T_1 is an important time scale for describing the relative growth of perturbations. Equation (39) applies for $T < T_1$ and describes algebraically decaying oscillations. However, relative to h_0 [which decays like $O(T^{-1})$], the relative amplitude of H is increasing; namely, we observe transient growth $H/h_0 = O(T^{1/4})$ for $T_0 \le T < T_1$.

This result can be made precise in terms of the specific form of the long-time asymptotics [Eq. (37)] corresponding to solution (39),

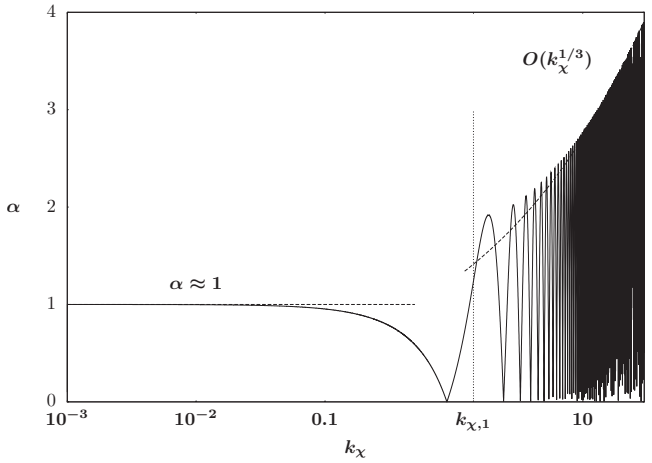

FIG. 5. The amplification factor $\alpha(k_\chi)$ for inviscid sheets with respect to 1D perturbations in the axial direction. Asymptotes for the short- and long-wave limits are shown by dashed lines.

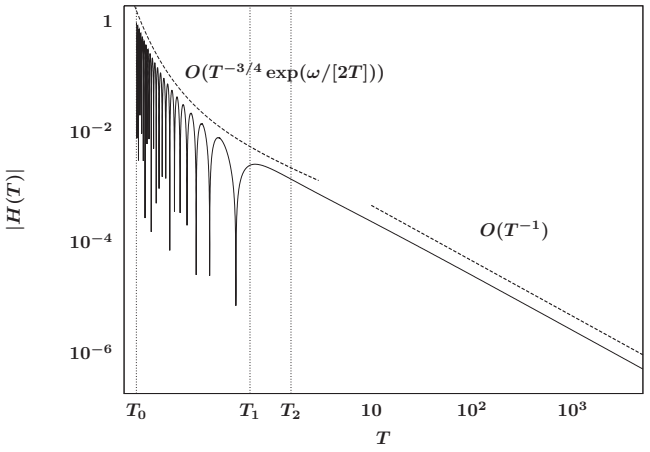

FIG. 6. Axial perturbations for the low viscosity case: Time evolution of the perturbation amplitude with transient and long-time asymptotes, Eqs. (45) and (44), respectively.

$$H(T) \sim \left[\frac{\sqrt{4\pi}\sin\left(\theta_0 + \frac{5\pi}{12} - \frac{2}{3}T_0^{-3/2}\right)T_0^{3/4}}{3^{2/3}\Gamma(2/3)\cos\theta_0}\right]\frac{1}{T} + O(T^{-2}), \quad T \to \infty. \tag{41}$$

Writing Eq. (41) in terms of τ, we obtain an upper bound on the long-time magnitude of the perturbations to the sheet thickness, for $\tau \to \infty$

$$|H_1(\tau)| \le \frac{\alpha}{\tau} \quad \text{with} \quad \alpha(k_\chi) = O(k_\chi^{1/3}\,\mathrm{We}^{-1/12}). \tag{42}$$

Note that $\alpha \to \infty$ as $k_\chi \to \infty$, as shown in Fig. 5. The minimum wavenumber for this regime is given by transforming the condition $T_0 < T_1$ into unscaled variables, i.e.,

$$k_\chi > k_{\chi,1} \equiv \left(\frac{\mathrm{We}}{T_1^3}\right)^{1/4} \approx 1.42\,\mathrm{We}^{1/4}. \tag{43}$$

Therefore initial perturbations of fixed amplitude and sufficiently short wavelength ($k_\chi \gg k_{\chi,1}$) can yield arbitrarily large deviations to the long-time sheet thickness. In contrast, if $k_\chi < k_{\chi,1}$ then perturbations are well described by Eq. (38) for all times and do not grow from their initial amplitude.

We interpret this short-wave instability as being driven by the competing effects of inertia and surface tension where increasing the effect of inertia relative to surface tension increases We and delays the instability to higher wavenumber. In the limit of high inertia relative to surface tension (We $\to \infty$), this transient growth mechanism [Eq. (42)] is absent for all wavenumbers $k_\chi < \infty$, and the sheet is marginally stable. Hence for finite We, inviscid sheets are weakly unstable [i.e., $\max_{k_\chi} \alpha(k_\chi) \to \infty$] to perturbations imposed in the axial direction.

This analysis of the time-dependent motion of an inviscid sheet to 1D axial perturbations uses a weaker definition of stability that distinguishes asymptotic marginal stability from instability through the transient growth parameter (or amplification factor) α rather than the typical normal-mode eigenvalue analysis which assumes exponential time dependence of the perturbation. As a result, direct comparison to other studies of infinite inviscid sheets[26,27] is not possible.

B. Viscous problem

For $\omega > 0$ Eq. (35) does not have a closed-form solution, but we can proceed with the stability analysis based on local asymptotics of its general solution. The local asymptotic expansion for the solutions of Eq. (35) for $T \to \infty$ is

$$H(T) \sim \frac{c_1}{T}\left[1 + \frac{\omega}{T} - \frac{1 - \frac{3}{2}\omega^3}{6T^3} - \frac{\omega \ln T}{T}\left(1 + \frac{\omega}{T} + \cdots\right)\right] + \frac{c_2}{T^2}\left(1 + \frac{\omega}{T} + \frac{\omega^2}{2T^2} - \frac{1 - 2\omega^3}{12T^3}\right). \tag{44}$$

Note that if $\omega = 0$, this solution reduces to Eq. (37), while the influence of finite viscosity is to add logarithmic and algebraic terms that yield small perturbations to Eq. (37) for $T \to \infty$. If the initial time T_0 is sufficiently large for Eq. (44) to apply, then $b_1 \sim T_0$, and like Eq. (38) we can conclude that $\alpha \approx 1$. Therefore, viscous long-wave perturbations ($k_\chi \to 0$) are marginally stable.

The influence of viscosity has a more interesting effect on short-wave perturbations ($k_\chi \to \infty$); since T_0 is inversely related to k_χ by Eq. (34), this corresponds to $T_0 \to 0$. Using the Wentzel-Kramers-Brillouin (WKB) theory,[58] we obtain the solution of Eq. (35) for $T \to 0$ to be

$$H(T) \sim \frac{(T/T_0)^{-3/4}}{\cos\theta_0}\exp\left(\frac{\omega}{2}\left[\frac{1}{T} - \frac{1}{T_0}\right]\right) \times \cos\left(\frac{2}{3}[T^{-3/2} - T_0^{-3/2}] - \frac{1}{4}\omega^2[T^{-1/2} - T_0^{-1/2}] + \theta_0\right), \tag{45}$$

where θ_0 is a phase parameter. If $\omega = 0$, then Eq. (45) reduces to Eq. (39). The time evolution of the perturbation amplitude $|H(T)|$ for a moderate value of k_χ is shown in Fig. 6.

We do not present a connection formula to relate the limiting behaviors for $T \to 0$ and $T \to \infty$ in this problem.

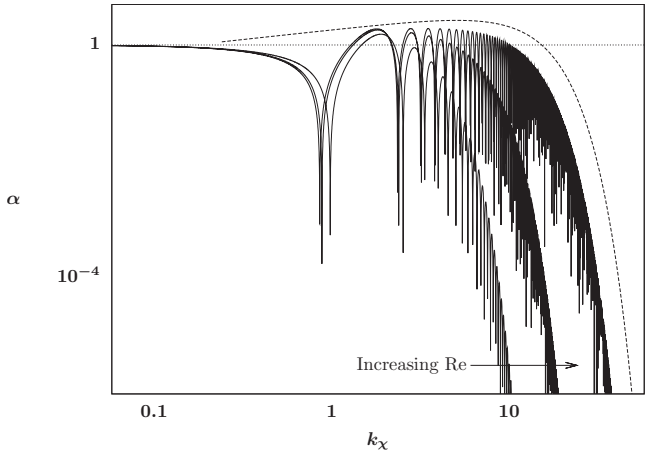

FIG. 7. Amplification factor for the low viscosity case with respect to 1D perturbations in the axial direction at several values of the Reynolds number. The analytical estimate [Eq. (47)] is shown as the dashed curve.

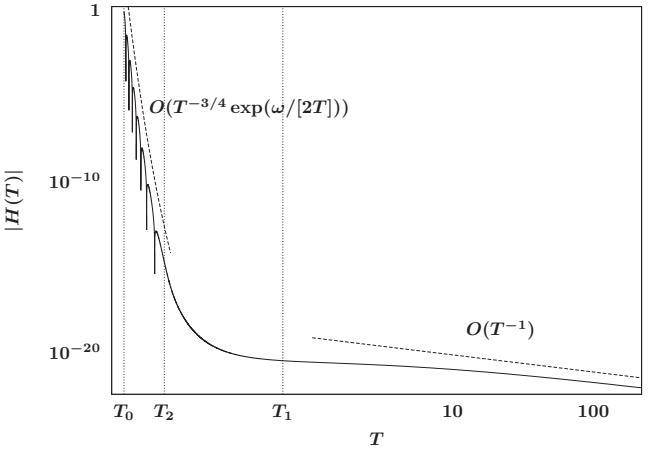

FIG. 8. Axial perturbations for the moderate viscosity case: Time evolution of the perturbation amplitude with asymptotic behaviors.

However, from a simple approximate patching argument by setting Eq. (45) equal to Eq. (28) at $T=T_1$, i.e., $H\sim\alpha T_0/T$, we find that the long-time behavior of the solution (45) for $T\to\infty$ obeys

$$|H(T)| \propto T_0^{3/4}\exp\left(-\frac{\omega}{2T_0}\right)\frac{1}{T}, \tag{46}$$

where the constant of proportionality should be independent of ω for $\omega\to 0$. Consequently we obtain the functional form of the amplification factor for large k_χ,

$$\alpha(k_\chi) \propto \frac{k_\chi^{1/3}}{\mathrm{We}^{1/12}}e^{-2k_\chi^2/\mathrm{Re}}. \tag{47}$$

This expression reduces to Eq. (42) for $\mathrm{Re}\to\infty$. The amplification factor is shown in Fig. 7. As before, for the transient behavior to be observed, the initial time must be small, $T_0<T_1$, given by condition (43). Note that for this case there is a finite range of wavenumbers where perturbations exhibit transient growth ($\alpha>1$) on $0<k_\chi<k_{\chi,2}$ where $k_{\chi,2}\approx O(\sqrt{\mathrm{Re}})$ as $\mathrm{Re}\to\infty$. As $\mathrm{Re}\to\infty$, the inviscid behavior is approached, but for any fixed value of Re, $\alpha(k_\chi)$ is uniformly bounded, as shown in Fig. 7. Consequently, we conclude that axial perturbations in the low but finite viscosity case are marginally stable.

The above discussion applies for $\omega\to 0$; our analysis shows that higher viscosity flows (with larger ω) will exhibit different behavior. For $\omega\to 0$, we can apply the argument used for Eq. (39) on Eq. (45) to estimate an upper bound on the time when oscillatory behavior ends as T_1, as given by Eq. (40). However, in the case of higher viscosity there is another consideration which can further limit the oscillations. Observe that the Liouville–Green transformation[58,59] can be applied to Eq. (35) to write it as a Schrödinger-type equation for $\tilde{H}(T)$ under the change of variables $H(T)=T^{-2}\tilde{H}(T)\exp(\frac{1}{2}\omega T^{-1})$,

$$\frac{d^2\tilde{H}}{dT^2}+\tilde{Q}(T)\tilde{H}=0, \quad \tilde{Q}(T)=\frac{1}{T^5}-\frac{\omega^2}{4T^4}-\frac{\omega}{T^3}. \tag{48}$$

If $\tilde{Q}(T)$ is positive for some T, then solutions will locally be oscillatory; otherwise solutions will exhibit nonoscillatory exponential growth/decay. In the inviscid case, $\tilde{Q}>0$ for all T. With finite viscosity, $\tilde{Q}(T)$ changes sign and becomes negative for large T, meaning that oscillations are only possible at short times. This defines a new characteristic time; let T_2 be the positive root of $\tilde{Q}(T_2)=0$,

$$T_2(\omega)=\frac{\sqrt{\omega^4+64\omega}-\omega^2}{8\omega}. \tag{49}$$

In terms of WKB analysis, T_2 is a first-order turning point of Eq. (48). If $T_2>T_1$, then the upper bound on the range of oscillatory behavior is set by T_1, as shown in Fig. 6, and we expect the solution to follow the analysis given by Eqs. (45)–(47). The condition $T_2>T_1$ gives a bound on the range for the "low viscosity" behavior in terms of ω,

$$0\le\omega<1.575. \tag{50}$$

In the high viscosity regime, where $T_2<T_1$, the relative sizes of T_0 versus T_2 become important in determining the dynamic behavior. The critical case where $T_0=T_2$ determines a critical wavenumber,

$$k_\chi^{\mathrm{osc}}=\sqrt{\frac{4\ \mathrm{Re}\ \mathrm{We}}{\mathrm{Re}^2-4\ \mathrm{We}}}, \tag{51}$$

namely, the amplitude of perturbations with $k_\chi>k_\chi^{\mathrm{osc}}$ will exhibit temporal oscillations at least for short times while longer waves will have monotonic decay. Taking $k_\chi^{\mathrm{osc}}\to\infty$ determines a critical Ohnesorge number, $\mathrm{Oh}\equiv\sqrt{\mathrm{We}}/\mathrm{Re}$, as $\mathrm{Oh}_c=1/2$, such that if $\mathrm{Oh}>\mathrm{Oh}_c$ then all perturbation modes have monotonic decay for all times.

In the case where $T_0<T_2<T_1$, the perturbations will exhibit rapid decaying oscillations until T_2, see Fig. 8. For large k_χ, the amplification factor should have the same general form as Eq. (47) though the constant of proportionality will reflect the further decay that occurs on the range T_2

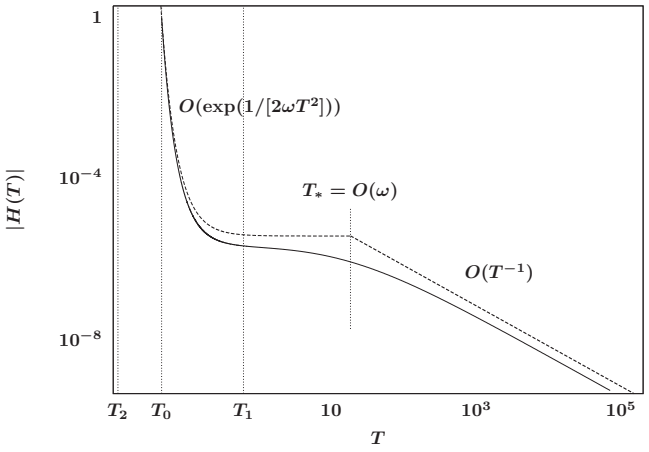

FIG. 9. Axial perturbations for the high viscosity case: Time evolution of the perturbation amplitude with asymptotic behaviors.

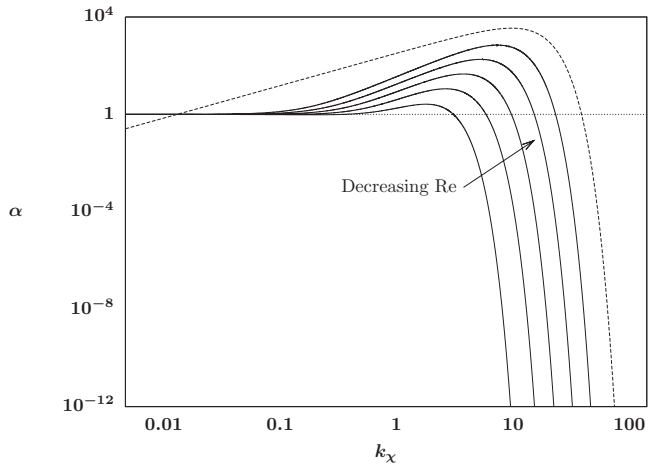

FIG. 10. Amplification factor for the high viscosity case with respect to 1D axial perturbations at several values of the Reynolds number (solid curves). The analytical estimate [Eq. (54)] is shown as the dashed curve. Note that for fixed We, decreasing the Reynolds number corresponds to increasing the capillary number.

$< T < T_1$. It is helpful to recall the parameter dependence of these times: T_0 depends only on the wavenumber and We [Eq. (34)], while T_1 is a pure constant [Eq. (40)], and T_2 reflects the influence of viscosity [Eq. (49)].

When $T_2 < T_0$ no oscillations will occur, as shown in Fig. 9. This is the case for short-wave perturbations in the high viscosity limit. The behavior of perturbations for short times with $T > T_0$ is obtained by considering Eq. (35) for large ω. Rescaling the solution as $H(T) = \bar{H}(\bar{T})$ with $T = \omega^{-1/2}\bar{T}$ transforms Eq. (35) to

$$\omega^{-3/2}\frac{d^2\bar{H}}{d\bar{T}^2} + \left(\frac{4\omega^{-3/2}}{\bar{T}} + \frac{1}{\bar{T}^2}\right)\frac{d\bar{H}}{d\bar{T}} + \left(\frac{2\omega^{-3/2}}{\bar{T}^2} + \frac{1}{\bar{T}^5}\right)\bar{H} = 0. \tag{52}$$

For $\omega \to \infty$, at leading order we get $\bar{H}(\bar{T}) \sim ce^{1/[2\bar{T}^2]} + O(\omega^{-3/2})$, or subject to the initial condition $H(T_0) = 1$,

$$H(T) \sim \exp\left(\frac{1}{2\omega}[T^{-2} - T_0^{-2}]\right) + O(\omega^{-1}), \tag{53}$$

for $T = O(1)$. The next term in the expansion of the solution of Eq. (52) for $\omega \to \infty$ includes a secular term of the form $\omega^{-1}TH(T)$. We conclude that the asymptotic expansion is only well ordered up to $T < T_* = O(\omega)$, as shown in Fig. 9. To obtain a connection to the long-time behavior we set Eq. (53) equal to $H = \alpha T_0/T$ at $T = T_*$, yielding

$$\alpha(k_\chi) \propto k_\chi^2 \exp\left(\frac{\mathrm{Re}}{128k_\chi^2\,\mathrm{We}}[\mathrm{Re}^2 - 16k_\chi^4]\right), \tag{54}$$

see Fig. 10. This result can be made more rigorous by regarding Eq. (52) as a singular perturbation problem with $\epsilon = \omega^{-3/2} \to 0$; then Eq. (54) is a consequence of leading order matching of Eq. (53) to the singular solution for $\bar{T} \to \infty$. It is somewhat unexpected that in this regime the maximum amplification factor increases with increasing viscosity; though other aspects of the behavior are more conventional: decreasing the influence of surface tension relative to viscous effects increases the range of wavenumbers with $\alpha(k_\chi) > 1$ on $0 < k_\chi < k_{\chi,3}$ with $k_{\chi,3} \approx O(\sqrt{\mathrm{We}/\mathrm{Re}})$ for $\mathrm{Re} \to 0$, or in terms of the capillary number, $\mathrm{Ca} = \mathrm{We}/\mathrm{Re}$, $k_{\chi,3} \approx O(\sqrt{\mathrm{Ca}})$ for $\mathrm{Ca} \to \infty$.

To summarize our results from this section we plot the maximum amplification factor at a given Reynolds number (with We held fixed), $\alpha_{\max}(\mathrm{Re}) = \max_{k_\chi} \alpha(k_\chi, \mathrm{Re})$, see Fig. 11. The numerical results plotted are obtained from scanning Figs. 7 and 10 over a range of Reynolds numbers. The asymptotic behaviors, $\alpha_{\max} = O(\mathrm{Re}^{1/6})$ for $\mathrm{Re} \to \infty$ and $\alpha_{\max} = O(\mathrm{Re}^{-2})$ for $\mathrm{Re} \to 0$, are obtained analytically from the critical points, i.e., $\partial_{k_\chi}\alpha = 0$, of Eqs. (47) and (54), respectively. In both of these limits, with the critical wavenumber being $k_\chi \to \infty$, the amplification factor is unbounded. Consequently, while at any finite Reynolds number, $\alpha_{\max}$ is bounded and the flow should be viewed as being marginally asymptotically stable. For Stokes flow and inviscid flow, axial short-wave perturbations can exhibit unbounded transient growth so that the sheet is weakly unstable.

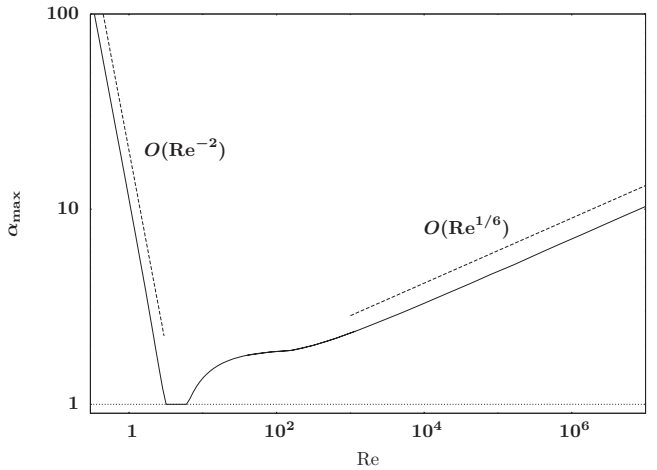

FIG. 11. Maximum amplification factor for 1D axial perturbations as a function of Reynolds number (for fixed We) with asymptotes derived from Eqs. (47) and (54).

VI. 1D PERTURBATIONS IN THE TRANSVERSE DIRECTION

We now consider the growth of spatial perturbations with structure solely in the direction transverse to the unperturbed flow. These perturbations will have $k_x=0$ and hence Eq. (24) reduces to

$$\frac{dH_1}{d\tau} = -\frac{H_1}{\tau} - \frac{ik_y}{\tau}V_1, \tag{55a}$$

$$\frac{dU_1}{d\tau} = -\frac{U_1}{\tau} - \frac{k_y^2}{\mathrm{Re}}U_1, \tag{55b}$$

$$\frac{dV_1}{d\tau} = -\frac{1}{\mathrm{Re}}(-2ik_yH_1 + 4k_y^2V_1) - \frac{ik_y^3}{\mathrm{We}}H_1. \tag{55c}$$

Noting that Eq. (55b) decouples from the rest of Eq. (55), and using the initial condition $U_1(1)=U^0$, the solution of Eq. (55b) is

$$U_1(\tau) = \frac{U^0}{\tau}e^{-k_y^2\,\mathrm{Re}^{-1}(\tau-1)}. \tag{56}$$

Consequently, $|U_1(\tau)|<|U^0|$ for all $\tau>1$ and we see that infinitesimal perturbations to u remain bounded by the initial disturbance amplitude for all times.

For the special case $k_y=0$, we obtain the marginally stable solution $H_1(\tau)=1/\tau$, $U_1(\tau)=U^0/\tau$, $V^1(\tau)=V^0$. For $k_y\neq 0$ the remaining coupled Eqs. (55a) and (55c) can be rescaled using

$$H_1(\tau)=H(T), \quad V_1(\tau)=\left(\frac{1}{k_y}\right)V(T), \quad \tau=\left(\frac{\mathrm{We}}{k_y^4}\right)T \tag{57}$$

to yield

$$\frac{dH}{dT} = -\frac{H}{T} - \frac{iV}{T}, \tag{58a}$$

$$\frac{dV}{dT} = -iH + \sigma(2iH - 4V), \tag{58b}$$

where the only remaining explicit parameter is

$$\sigma = \frac{\mathrm{We}}{k_y^2\,\mathrm{Re}}. \tag{59}$$

Note that σ is closely related to the capillary number, $\mathrm{Ca}=\mathrm{We}/\mathrm{Re}$. The initial condition is normalized as in Sec. V to be

$$H(T_0)=1 \quad \text{at} \quad T_0=\frac{k_y^4}{\mathrm{We}}, \tag{60}$$

where H will be real-valued for all times if V is pure imaginary. As in the case of axial perturbations, the remaining first-order system (58a) and (58b) can be combined into a second-order equation for $H(T)$,

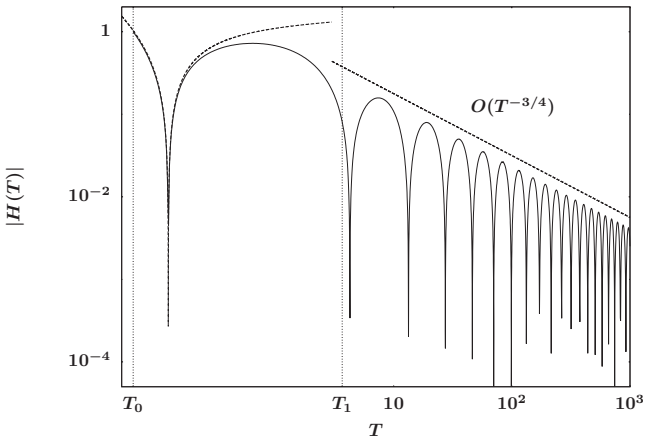

FIG. 12. Transverse perturbations for the inviscid case: Evolution of perturbation amplitude [Eq. (62)] showing transition from transient behavior [Eq. (63)] to $O(T^{-3/4})$ long-time behavior [Eq. (64)].

$$\frac{d^2H}{dT^2} + \left(\frac{2}{T}+4\sigma\right)\frac{dH}{dT} + \left(\frac{2\sigma+1}{T}\right)H = 0. \tag{61}$$

Like axial perturbations, distinctions between transient and long-time behaviors will occur for this problem with the exception that for transverse perturbations, asymptotic stability will have a clear dependence on the value of σ.

A. Inviscid problem

The inviscid problem ($\mathrm{Re}=\infty$) is given by setting $\sigma=0$ in Eq. (61). The reduced equation can be solved exactly in terms of Bessel functions of order 1, yielding

$$H(T) = [a_1Y_1(2\sqrt{T}) + a_2J_1(2\sqrt{T})]T^{-1/2}. \tag{62}$$

As in Sec. V, having a closed-form exact solution allows us to completely analyze stability for this case.

The asymptotic form of Eq. (62) valid for $T\to 0$ is

$$H(T) \sim b_1\left(\frac{1}{T} - \ln T + (2\gamma-1)\right) + b_2\left(1 - \frac{1}{2}T + \frac{1}{12}T^2\right), \tag{63}$$

where $\gamma\approx 0.577\,215$ is the Euler–Mascheroni constant. For sufficiently small T_0, applying the initial condition $H(T_0)=1$ to Eq. (63) yields $b_1\sim T_0$. This transient behavior for $T\to 0$, shown in Fig. 12, applies only briefly before the perturbations approach the form set by the long-time asymptotics.

For $T\to\infty$, Eq. (62) is a decaying oscillatory solution. If T_0 is sufficiently large, then applying the initial condition (60) to the asymptotic form of Eq. (62) valid for $T\to\infty$ yields

$$H(T) \sim \frac{(T/T_0)^{-3/4}}{\cos\,\theta_0}\cos(2[\sqrt{T}-\sqrt{T_0}]+\theta_0), \tag{64}$$

where θ_0 is a phase constant, see Fig. 12. In contrast to the dynamics of axial perturbations, here the oscillatory behavior occurs for long times instead of short times.

Notice in Fig. 12 that $H(T)$ transitions to $O(T^{-3/4})$ behavior after the first complete period of oscillation (i.e., near the second zero). In particular, an upper bound for the transition

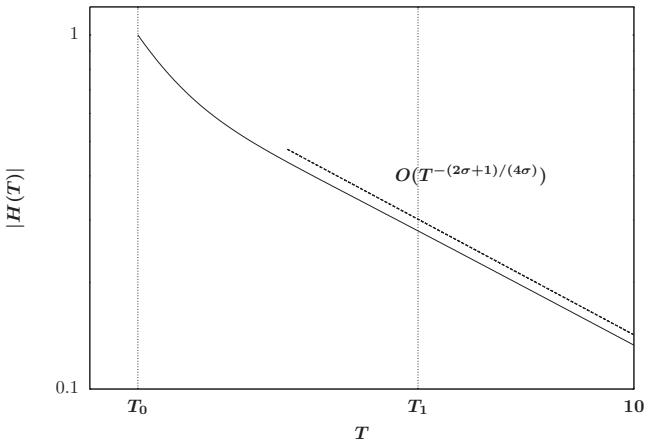

FIG. 13. Evolution of the amplitude of a transverse perturbation for $\sigma=1$; Eq. (66) gives the long-time asymptotics.

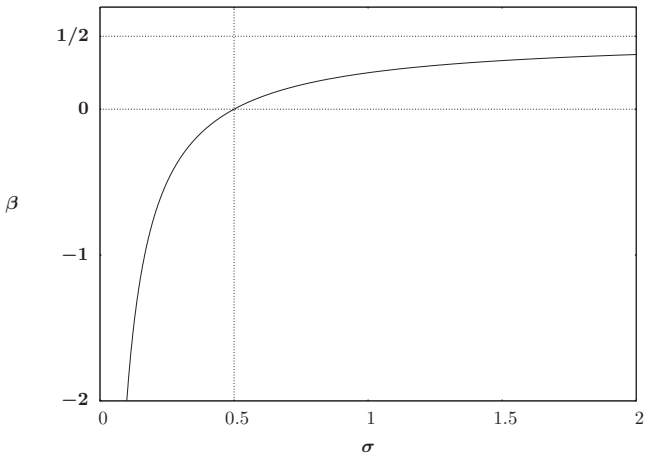

FIG. 14. Asymptotic growth rate of transverse perturbations $\beta(\sigma)$ showing the change in stability at $\sigma=\frac{1}{2}$.

time T_1 is related to the maximum value of the first zero of $a_1Y_1(S_1)+a_2J_1(S_1)$ over all possible a_1, a_2, yielding $S_1 \approx 3.8317$. This sets a time scale that defines the end of transient behavior,

$$T_1 \leq \left(\frac{S_1}{2}\right)^2 \approx 3.6704, \tag{65}$$

with the transient behavior [Eq. (63)] applying while $T_0 \leq T < T_1$.

While the scaling amplitude of the perturbation depends on the relative size of T_0 versus T_1, for sufficiently long times ($T_1 \gg T_0$) the solution will evolve according to Eq. (64) for all $k_y > 0$. Consequently, these perturbations will grow relative to the base state as $H/h_0 = O(T^{1/4})$ and we conclude that inviscid sheets are asymptotically unstable to transverse perturbations.

B. Viscous problem

For $\sigma > 0$, Eq. (61) has a closed-form solution for $H(T)$ in terms of the Kummer special functions[60] but since the properties of these confluent hypergeometric functions are somewhat opaque, we will avoid using them. In the limit $T \to 0$, the solution can be written as a Frobenius series, of similar qualitative form to Eq. (63). For $T \to \infty$, we obtain the asymptotic expansion of the solution of Eq. (61) via WKB analysis as

$$H(T) \sim c_1 T^{-(2\sigma+1)/4\sigma} \exp\left(\frac{1-4\sigma^2}{64\sigma^2 T}\right) + c_2 T^{(1-6\sigma)/4\sigma} e^{-4\sigma T}. \tag{66}$$

For long times the first term will always eventually dominate, but for short to moderate times the second term could be of competing size if $\sigma > \frac{1}{2}$. Figure 13 shows this behavior for $\sigma=1$ with $|H| = O(T^{-(2\sigma+1)/(4\sigma)})$ for $T \to \infty$. Equation (66) allows us to directly define the long-time asymptotic growth rate of perturbations relative to the base flow as $|H_1(\tau)/h_0(\tau)| = O(\tau^\beta)$, or equivalently,

$$\beta \equiv \lim_{\tau\to\infty} \frac{\ln|H_1(\tau)/h_0(\tau)|}{\ln \tau} = \frac{2\sigma-1}{4\sigma} = \frac{1}{2} - \frac{k_y^2\,\mathrm{Re}}{4\,\mathrm{We}}, \tag{67}$$

as shown in Fig. 14. The sheet is asymptotically stable if $\beta < 0$ and unstable if $\beta > 0$. The condition for asymptotic stability, which is equivalent to $\sigma < \frac{1}{2}$, can also be written as

$$k_y > \sqrt{2\,\mathrm{Ca}}, \tag{68}$$

i.e., the capillary number sets a critical wavenumber. However, reconciling this prediction for inviscid sheets, $\beta(\sigma \to 0) \to -\infty$ from Eq. (66) versus $\beta(\sigma=0)=\frac{1}{4}$ from Eq. (64), requires analysis of the transient behavior which we address next.

For $\sigma < \frac{1}{2}$, a second time scale T_2 is set that determines whether transient oscillatory behavior will occur. The change of variables $H(T) = T^{-1}\tilde{H}(T)e^{-2\sigma T}$ reduces Eq. (61) to

$$\frac{d^2\tilde{H}}{dT^2} + \tilde{Q}(T)\tilde{H} = 0, \quad \tilde{Q}(T) = \frac{1-2\sigma}{T} - 4\sigma^2. \tag{69}$$

Recall that if $\tilde{Q}(T) > 0$ for some T, then solutions will be locally oscillatory; otherwise solutions will exhibit exponential growth or decay. In the inviscid case, $\tilde{Q}(T) > 0$ for all T. For finite viscosity, $\tilde{Q}(T)$ changes sign and becomes negative for large T, so that oscillations are possible only up to a finite time. This defines the characteristic time T_2,

$$T_2(\sigma) = \frac{1-2\sigma}{4\sigma^2}, \tag{70}$$

which is positive if $0 < \sigma < \frac{1}{2}$. In this case, oscillations are possible for $T_0 \leq T < T_2$, though the behavior of the solution depends on the relative size of T_2 to T_1 [given by Eq. (65)] with the critical value, $\sigma_c \approx 0.2016$, defined by the condition $T_2 = T_1$.

For $\sigma_c < \sigma < \frac{1}{2}$ (i.e., $T_2 < T_1$), the solution may exhibit a single sign change [as indicated by a cusp with $|H| \to 0$ in the log-scale plots of $|H(T)|$] before converging to the long-time behavior [Eq. (66)], as shown in Fig. 15. The lower bound on T_2, given by $T_0 = T_2$, sets a critical wavenumber [similar to Eq. (51)]

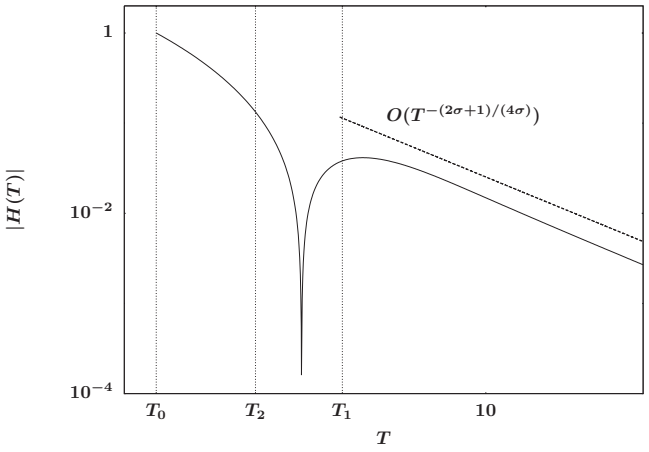

FIG. 15. Evolution of the transverse perturbation amplitude in the moderate capillary number case, here with $\sigma=\frac{1}{4}$.

$$k_y^{\mathrm{osc}} = \sqrt{\frac{2\ \mathrm{Re}\ \mathrm{We}}{\mathrm{Re}^2 - 4\ \mathrm{We}}}, \tag{71}$$

such that perturbations with $k_y < k_y^{\mathrm{osc}}$ or $\mathrm{Oh} > \frac{1}{2}$ exhibit monotonic decay, as in Sec. V B.

For $0<\sigma<\sigma_c$ (i.e., $T_2>T_1$), the perturbation amplitude will have many sign changes if T_2 is large, as shown in Fig. 16. Returning to Eq. (61), the limit $\sigma\to 0$ is a regular perturbation of the inviscid problem; therefore the solution should be of the form $H=H_{(0)}(T)+O(\sigma)$ where $H_{(0)}$ is the inviscid solution (62). Going to next order yields a secular term of the form $\sigma T H_{(0)}(T)$; hence the expansion is not uniformly valid for long times and the nearly inviscid behavior can only hold for $T<T_*=O(\sigma^{-1})$. Relative to the base solution, this yields transient growth, akin to the unstable behavior [Eq. (64)] in Sec. VI A. For long times, the solution will have rapid decay as given by Eq. (66) with $\beta\to-\infty$. These two regimes are connected through local analysis of the turning point problem for Eq. (69) at T_2, see Ref. 58. If we neglect this connection problem, we can still obtain a reasonable estimate by patching the asymptotic behaviors [Eqs. (64) and (66)] together at T_*, as shown in Fig. 16. This determines the coefficient in Eq. (66) to be $c_1 \approx O(\sigma^{-1/[4\sigma]}) \to \infty$ as $\sigma\to 0$, namely, the transient growth puts a very large prefactor on the long-time behavior. The consequence is that while for $T\to\infty$, perturbations for $\sigma\to 0$ will be seen to eventually decay, the influence of the initial growth will be to produce perturbations that can be very large at finite times, akin to the long-time unstable behavior for inviscid sheets at $\sigma=0$.

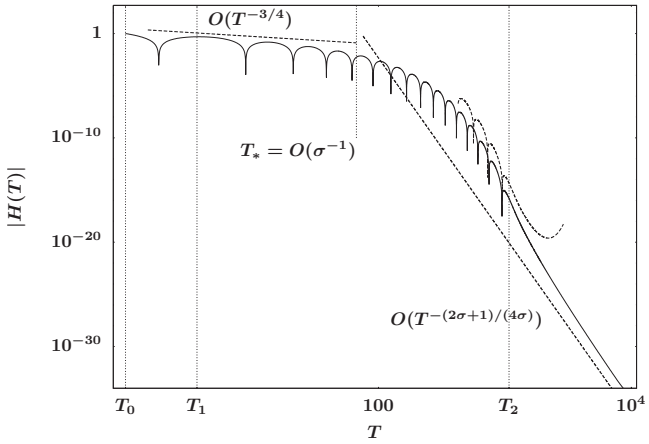

FIG. 16. Evolution of transverse perturbations for $\sigma\to 0$. Dashed curves show predictions for the moderate-time nearly inviscid behavior [Eq. (64)], the connection problem at T_2, and the long-time viscous decay [Eq. (66)].

In summary, while the asymptotic stability of viscous sheets is given by Eq. (67), we find that in the case of nearly inviscid sheets ($\sigma\to 0$), unstable transient growth of transverse perturbations can have a significant influence for finite times; in particular, these perturbations grow relative to the base state as $H/h_0 \sim O(T^{1/4})$. From Eq. (68), we find that viscous sheets will be asymptotically unstable to long-wave transverse perturbations for finite capillary numbers.

VII. STABILITY OF A SHEET TO 2D PERTURBATIONS

Having separately considered pure axial perturbations ($k_y=0$) and pure transverse perturbations ($k_\chi=0$), we return to the full system (24a)–(24c) to examine oblique perturbations with $k_\chi, k_y \neq 0$. It is convenient to rescale the Fourier coefficients in Eq. (24) using

$$H_1(\tau) = H(T), \quad U_1(\tau) = \left(\frac{1}{k_y}\right) U(T),$$

$$V_1(\tau) = \left(\frac{1}{k_y}\right) V(T), \quad \tau = \left(\frac{k_\chi}{k_y}\right) T, \tag{72}$$

yielding the governing ODEs

$$\frac{dH}{dT} = -\frac{H}{T} - \frac{iU}{T^2} - \frac{iV}{T}, \tag{73a}$$

$$\frac{dU}{dT} = -\frac{U}{T} - \psi\left(-\frac{4iH}{T} + \frac{4U}{T^2} + \frac{3V}{T} + U\right) - i\phi\left(\frac{1}{T^3} + \frac{1}{T}\right)H, \tag{73b}$$

$$\frac{dV}{dT} = -\psi\left(-2iH + \frac{V}{T^2} + \frac{3U}{T} + 4V\right) - i\phi\left(\frac{1}{T^2} + 1\right)H, \tag{73c}$$

with the two control parameters

$$\psi = \frac{k_\chi k_y}{\mathrm{Re}}, \quad \phi = \frac{k_\chi k_y^3}{\mathrm{We}}, \tag{74}$$

and the initial condition (30) becomes

$$H(T_0) = 1 \quad \text{at} \quad T_0 = \frac{k_y}{k_\chi}, \tag{75}$$

where, as in the previous cases (and without significant loss of generality), we take H to be real-valued with the velocity components being pure imaginary. For connection with the parameters used in previous sections, $\omega = 4\psi/\phi^{1/3}$, see Eq. (33), and $\sigma = \psi/\phi$, see Eq. (59). While it can be expected that Eqs. (73a)–(73c) encompass a richer set of dynamics than either of the 1D cases, we will not consider this exhaustively.

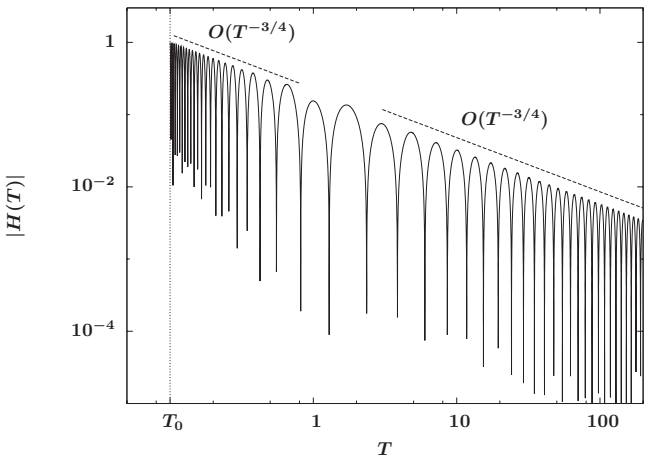

FIG. 17. Evolution of the amplitude for 2D perturbations of an inviscid sheet. Dashed lines show predicted decay rates for transient [Eq. (78)] and long-time [Eq. (80)] behaviors.

Rather, we will focus on the dominant behaviors and make connections to the related 1D behaviors developed earlier.

A. Inviscid problem

The stability problem for an inviscid sheet is obtained by setting $\psi=0$ in Eq. (73). The three coupled ODEs can be combined into a single third-order equation for $H(T)$,

$$\frac{d^3H}{dT^3}+\frac{6}{T}\frac{d^2H}{dT^2}+\left(\frac{6}{T^2}+\phi\frac{(1+T^2)^2}{T^5}\right)\frac{dH}{dT}+3\phi\left(\frac{1}{T^2}-\frac{1}{T^6}\right)H=0. \tag{76}$$

This equation has irregular singular points at both $T=0$ and $T=\infty$ and hence we can use WKB analysis to obtain asymptotic behaviors in both limits.

For $T\to 0$, we obtain

$$H(T)\sim a_1T^{-3/4}\cos\left(\tfrac{2}{3}\sqrt{\phi}T^{-3/2}+\theta_0\right)+a_2T^3e^{-3T^2}, \tag{77}$$

where a_1, a_2, θ_0 depend on the initial conditions. The decaying oscillatory term dominates the transient behavior. Note that rescaling Eq. (77) into the original variables yields

$$H_1(\tau)\approx O\left(\tau^{-3/4}\cos\left[\tfrac{2}{3}k_\chi^2\,\mathrm{We}^{-1/2}\,\tau^{-3/2}\right]\right), \tag{78}$$

as shown in Fig. 17; this is equivalent to Eq. (39) from Sec. V A. Therefore, we conclude that the transient behavior of general perturbations to inviscid sheets is dominated by the growth of perturbations in the axial component k_χ. The dependence of the solution for $T\to 0$ on k_y is weak since it does not enter at leading order.

Similarly, for $T\to\infty$, we obtain

$$H(T)\sim b_1T^{-3/4}\cos(2\sqrt{\phi T}+\theta_1)+b_2T^{-3}e^{-6/[\phi T]}, \tag{79}$$

with constants b_1, b_2, θ_1. Again, the decaying oscillatory behavior dominates and the unscaled long-time solution will take the form

$$H_1(\tau)\approx O(\tau^{-3/4}\cos[2k_y^2\,\mathrm{We}^{-1/2}\,\tau^{1/2}]), \tag{80}$$

as shown in Fig. 17; this is equivalent to Eq. (64) from Sec. VI A. Consequently, the long-time behavior of general perturbations to inviscid sheets is dominated by the growth of perturbations in the transverse component k_y. For $T\to\infty$, the dependence of the solution on k_χ is weak since it does not enter at leading order.

From the transient and long-time behaviors, we see that the unstable relative growth $|H_1/h_0|=O(\tau^{1/4})$ is maintained for all times; what differs is the form of the oscillatory behavior and whether the influence of the axial [Eq. (78)] or transverse [Eq. (80)] perturbations dominate. Given the form of Eqs. (78) and (80), we conclude that an inviscid sheet is unstable to general symmetric perturbations of all positive wavelengths.

B. Viscous problem

Finally, we consider general perturbations on a viscous sheet. As in the previous section, the viscous version of Eqs. (73a)–(73c) can be combined to form a linear third-order ODE for $H(T)$. The expressions for the coefficients make the equation somewhat long and cumbersome, so we will not write it out; for $\psi=0$ it reduces to Eq. (76). As in the previous section, we obtain the asymptotic behaviors for $H(T)$ from WKB analysis; we have also obtained the asymptotic behaviors for H, U, V directly from Eqs. (73a)–(73c) using the method of asymptotic partitioning given by Ref. 61.

For $T\to 0$, we find

$$H(T)\sim c_1T^{-3/4}e^{2\psi/T}\cos\left(\tfrac{2}{3}\sqrt{\phi}T^{-3/2}-4\psi^2\phi^{-1/2}T^{-1/2}+\theta_0\right)+c_2T^3e^{\psi/T}, \tag{81}$$

with constants c_1, c_2, θ_0. Putting the dominant behavior in original variables yields

$$H_1(\tau)\approx O\left(\tau^{-3/4}e^{2k_\chi^2/(\tau\,\mathrm{Re})}\cos\left[k_\chi^2\,\mathrm{We}^{-1/2}\left(\tfrac{2}{3}\tau^{-3/2}-4\,\mathrm{We}\,\mathrm{Re}^{-2}\,\tau^{-1/2}\right)\right]\right); \tag{82}$$

this is equivalent to the transient viscous behavior for axial perturbations [Eq. (45)]. As in the 2D inviscid case, the transient behavior is independent of k_y to leading order.

For $T\to\infty$, we obtain

$$H(T)\sim d_1T^{-(\phi+2\psi)/(4\psi)}+d_2T^{(\phi-6\psi)/(4\psi)}e^{-4\psi T}+d_3T^{-4}e^{-\psi T}, \tag{83}$$

with constants d_1, d_2, d_3. For $\psi>0$, the second and third modes exponentially decay; hence the first mode is the dominant long-time behavior, which in original variables is given by

$$H_1(\tau)\approx O(\tau^{-(1/2)-k_y^2\,\mathrm{Re}/[4\,\mathrm{We}]}); \tag{84}$$

this is the same as the long-time behavior of Eq. (66). As in the 2D inviscid case, the long-time behavior is independent of k_χ to leading order. Figure 18 shows a numerically computed solution of Eqs. (73a)–(73c) compared with the transient [Eq. (81)] and long-time [Eq. (83)] asymptotic behaviors. Note that some caution must be used, as the same transitions in qualitative behaviors for different parameter ranges that were observed in Secs. V B and VI B will occur here.

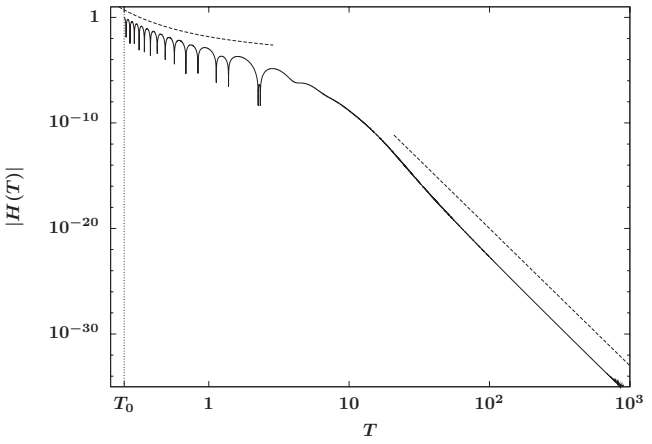

FIG. 18. Evolution of the amplitude for 2D perturbations of a viscous sheet. Dashed lines show predicted decay rates for transient [Eq. (81)] and long-time [Eq. (83)] behaviors.

Examining $|H_1/h_0|$ to determine whether the perturbations grow or decay relative to the base solution, we find that the condition for asymptotic stability is

$$k_y > \sqrt{2\mathrm{We}/\mathrm{Re}} = \sqrt{2\ \mathrm{Ca}}, \tag{85}$$

which is the same condition as Eq. (68). Hence, the asymptotic stability of the sheet is controlled by the transverse component of the symmetric perturbations, in particular, for any finite Ca the sheet is unstable to long-wave transverse perturbations.

VIII. CONCLUSIONS

Using the full Navier–Stokes equations we have derived a time-dependent exact solution for the idealized extensional motion of an incompressible planar sheet driven by inertia. The solution, which includes a balance of inertial, gravitational, and viscous effects, requires no *a priori* assumptions on the thickness of the sheet, is valid for any value of the acceleration due to gravity and any value for the viscosity, and is independent of the value of the surface tension.

The exact solution also satisfies the long-wave model for a long, thin liquid sheet. We examine the linear stability of our time-dependent exact solution within the framework of the long-wave model to 1D and 2D symmetric perturbations imposed in the axial and transverse directions for viscous and inviscid fluids. Both transient growth and long-time asymptotic stability were considered. Owing to the time dependence of the exact solution, the stability analysis involves solving an initial value problem instead of a standard normal-mode eigenvalue problem. Consequently, our predictions for stability are determined based on the time-dependent growth of perturbations relative to the base solution. In some of the cases considered, we find that transient effects can influence the long-time stability of the sheet which motivated our study of both transient and long-time stability.

For 1D perturbations in the axial direction, inviscid and viscous sheets are asymptotically marginally stable, though we find that transient growth can have an important effect and depends on the values of the Weber and Reynolds numbers. In particular, for these two cases our results use a weaker definition of stability that distinguishes asymptotic marginal stability from instability through a transient growth parameter (or amplification factor) α. Though the geometry of the problem makes it tempting to compare our results with temporal stability studies for symmetric perturbations on inviscid sheets and curtains,[26–28,35] this must be avoided. While it is generally true that the Reynolds and Weber numbers are the key parameters, the differences between our results and these classical studies is significant. Our base flow is time-dependent and extensional, while theirs is steady and unidirectional. The results of the other studies are derived from coupling the motion of the sheet to that of the surrounding gas, whereas we have neglected the influence of the surrounding gas taking it to have negligible density compared to that of the sheet. Finally, since our results for axial perturbations can involve large transient deviations from the delicate case of marginal linear stability, it is highly likely that nonlinear effects will play an important role. Consequently, further studies are needed to conclusively determine the expected behavior for purely axial perturbations to extensional sheets.

Some precedent for the dynamics we describe is given in an analogous study by Frankel and Weihs[6] who considered the stability of viscous stretching jets. Similar to our problem, their solution is time-dependent and their stability analysis involves the study of transient and long-time behaviors. As in our results from Sec. V B, they observed the "dual" role of viscosity in amplifying transient growth (which they attribute to the axial viscous force) before yielding to the more classical damping expected for long times. Likewise, they obtained perturbations that had oscillatory transient behavior before transitioning to long-time monotonic decay, as in our Figs. 6, 8, 16, and 18.

Returning to our results, we find that inviscid sheets are asymptotically unstable to 1D transverse perturbations of all wavelengths. Hence, in terms of 1D perturbations, transverse perturbations may be regarded as more dangerous to the stability of an inviscid sheet than axial ones. For general 2D perturbations, inviscid sheets are unstable to perturbations of all wavelengths with the transient dynamics controlled by axial perturbations and the long-time dynamics controlled by transverse perturbations. The asymptotic stability of viscous sheets to 1D transverse perturbations and to general 2D perturbations is dependent on the capillary number. In both cases, the sheet is asymptotically unstable to long-wave transverse perturbations at any finite Ca, such that decreasing the influence of surface tension relative to viscosity increases the range of unstable wavenumbers. This observation, that surface tension acts to stabilize the motion of a sheet, has been illustrated in other types of sheet flows.[26,27]

ACKNOWLEDGMENTS

L.B.S. acknowledges support from NSF Grant No. DMS-0707755. T.P.W. acknowledges support from NSF Grant Nos. DMS-0239125 CAREER and DMS-0244498 FRG. Both authors gratefully acknowledge the Distinguished

Visiting Professor Program in the Mathematics Department at Bucknell University for supporting their collaborative efforts.

[1]J. E. Matta and R. P. Tytus, "Liquid stretching using a falling cylinder," J. Non-Newtonian Fluid Mech. **35**, 215 (1990).
[2]T. Sridhar, V. Titaatmadja, D. A. Nguyen, and R. K. Gupta, "Measurement of extensional viscosity of polymer solutions," J. Non-Newtonian Fluid Mech. **40**, 271 (1991).
[3]G. H. McKinley and T. Sridhar, "Filament-stretching rheometry of complex fluids," Annu. Rev. Fluid Mech. **34**, 375 (2002).
[4]H. Matallah, K. S. Sujatha, M. J. Banaai, and M. F. Webster, "Single and multi-mode modelling for filament stretching flows," J. Non-Newtonian Fluid Mech. **146**, 92 (2007).
[5]I. Frankel and D. Weihs, "Stability of a capillary jet with linearly increasing axial velocity (with applications to shaped charges)," J. Fluid Mech. **155**, 289 (1985).
[6]I. Frankel and D. Weihs, "Influence of viscosity on the capillary instability of a stretching jet," J. Fluid Mech. **185**, 361 (1987).
[7]D. M. Henderson, H. Segur, L. B. Smolka, and M. Wadati, "The motion of a falling liquid filament," Phys. Fluids **12**, 550 (2000).
[8]L. B. Smolka, A. Belmonte, D. M. Henderson, and T. P. Witelski, "Exact solution for the extensional flow of a viscoelastic filament," Eur. J. Appl. Math. **15**, 679 (2004).
[9]D. H. Peregrine, G. Shoker, and A. Symon, "The bifurcation of liquid bridges," J. Fluid Mech. **212**, 25 (1990).
[10]X. D. Shi, M. P. Brenner, and S. R. Nagel, "A cascade of structure in a drop falling from a faucet," Science **265**, 219 (1994).
[11]R. M. S. M. Schulkes, "The evolution and bifurcation of a pendant drop," J. Fluid Mech. **278**, 83 (1994).
[12]X. Zhang and O. A. Basaran, "An experimental study of dynamics of drop formation," Phys. Fluids **7**, 1184 (1995).
[13]D. M. Henderson, W. G. Pritchard, and L. B. Smolka, "On the pinch-off of a pendant drop of viscous fluid," Phys. Fluids **9**, 3188 (1997).
[14]J. Eggers, "Nonlinear dynamics and breakup of free-surface flows," Rev. Mod. Phys. **69**, 865 (1997).
[15]E. D. Wilkes, S. D. Phillips, and O. A. Basaran, "Computational and experimental analysis of dynamics of drop formation," Phys. Fluids **11**, 3577 (1999).
[16]L. B. Smolka, "On the motion of Newtonian and non-Newtonian liquid filaments: Stretching, beading, blistering, pinching," Ph.D. thesis, Pennsylvania State University, 2002.
[17]Y. M. Stokes, E. O. Tuck, and L. W. Schwartz, "Extensional fall of a very viscous fluid drop," Q. J. Mech. Appl. Math. **53**, 565 (2000).
[18]Y. M. Stokes and E. O. Tuck, "The role of inertia in extensional fall of a viscous drop," J. Fluid Mech. **498**, 205 (2004).
[19]P. G. Drazin and W. H. Reid, *Hydrodynamic Stability* (Cambridge University Press, Cambridge, 2004).
[20]G. I. Taylor, "The dynamics of thin sheets of fluid. III. Disintegration of fluid sheets," Proc. R. Soc. London, Ser. A **253**, 313 (1959).
[21]C. Clanet and J. C. Lasheras, "Transition from dripping to jetting," J. Fluid Mech. **383**, 307 (1999).
[22]D. R. Brown, "A study of the behaviour of a thin sheet of moving liquid," J. Fluid Mech. **10**, 297 (1961).
[23]J. I. Ramos, "Planar liquid sheets at low Reynolds numbers," Int. J. Numer. Methods Fluids **22**, 961 (1996).
[24]S. J. Weinstein, A. Clarke, A. G. Moon, and E. A. Simister, "Time-dependent equations governing the shape of a two-dimensional liquid curtain, Part 1: Theory," Phys. Fluids **9**, 3625 (1997).
[25]L. De Luca, "Experimental investigation of the global instability of plane sheet flows," J. Fluid Mech. **399**, 355 (1999).
[26]H. B. Squire, "Investigation of the instability of a moving liquid film," Br. J. Appl. Phys. **4**, 167 (1953).
[27]W. W. Hagerty and J. F. Shea, "A study of the stability of plane fluid sheets," J. Appl. Mech. **22**, 509 (1955).
[28]X. Li and R. S. Tankin, "On the temporal instability of a two-dimensional liquid sheet," J. Fluid Mech. **226**, 425 (1991).
[29]S. P. Lin, "Stability of a viscous liquid curtain," J. Fluid Mech. **104**, 111 (1981).
[30]X. Li, "Spatial instability of plane liquid sheets," Chem. Eng. Sci. **48**, 2973 (1993).
[31]S. P. Lin, Z. W. Lian, and B. J. Creighton, "Absolute and convective stability of a liquid sheet," J. Fluid Mech. **220**, 673 (1990).
[32]S. P. Lin, *Breakup of Liquid Sheets and Jets* (Cambridge University Press, Cambridge, 2003).
[33]S. G. Chuech, "Spatial instability of a viscous liquid sheet," Int. J. Numer. Methods Fluids **50**, 1461 (2006).
[34]Y. L. Yeow, "On the stability of extending films: A model for the film casting process," J. Fluid Mech. **66**, 613 (1974).
[35]W. A. Sirignano and C. Mehring, "Review of theory of distortion and disintegration of liquid streams," Prog. Energy Combust. Sci. **26**, 609 (2000).
[36]C. Mehring and W. A. Sirignano, "Nonlinear capillary wave distortion and disintegration of thin planar liquid sheets," J. Fluid Mech. **388**, 69 (1999).
[37]N. Le Grand-Piteira, P. Brunet, L. Lebon, and L. Limat, "Propagating wave pattern on a falling liquid curtain," Phys. Rev. E **74**, 026305 (2006).
[38]P. J. Schmid and D. S. Henningson, "On the stability of a falling liquid curtain," J. Fluid Mech. **463**, 163 (2002).
[39]W. Minoshima and J. L. White, "Multiaxial elongational flow of sheets and annular cylinders: Growth of disturbances," J. Non-Newtonian Fluid Mech. **11**, 127 (1982).
[40]S. F. Han and E. Becker, "Hydrodynamic instability of extensional flows," Rheol. Acta **22**, 521 (1983).
[41]L. A. Romero, "The stability of stretching and accelerating plastic sheets," J. Appl. Phys. **69**, 7474 (1991).
[42]G. I. Taylor, "The dynamics of thin sheets of fluid. II. Waves on fluid sheets," Proc. R. Soc. London, Ser. A **253**, 296 (1959).
[43]M. Renardy, *Mathematical Analysis of Viscoelastic Flows* (Society for Industrial and Applied Mathematics, Philadelphia, 2000).
[44]J.-M. Chomaz, "The dynamics of a viscous soap film with soluble surfactant," J. Fluid Mech. **442**, 387 (2001).
[45]J. Eggers, "Nonlinear dynamics and breakup of free-surface flows," Rev. Mod. Phys. **69**, 865 (1997).
[46]T. Erneux and S. H. Davis, "Nonlinear rupture of free films," Phys. Fluids A **5**, 1117 (1993).
[47]D. Vaynblat, J. R. Lister, and T. P. Witelski, "Rupture of thin viscous films by van der Waals forces: Evolution and self-similarity," Phys. Fluids **13**, 1130 (2001).
[48]J. N. Dewynne and P. Wilmott, "Slender axisymmetric fluid jets," Math. Comput. Modell. **18**, 69 (1993).
[49]J.-M. Chomaz, "Global instabilities in spatially developing flows: Non-normality and nonlinearity," Annu. Rev. Fluid Mech. **37**, 357 (2005).
[50]P. J. Schmid and D. S. Henningson, *Stability and Transition in Shear Flows* (Springer-Verlag, New York, 2001).
[51]B. F. Farrell and P. J. Ioannou, "Generalized stability theory. II. Nonautonomous operators," J. Atmos. Sci. **53**, 2041 (1996).
[52]A. L. Bertozzi and M. P. Brenner, "Linear stability and transient growth in driven contact lines," Phys. Fluids **9**, 530 (1997).
[53]B. F. Farrell and P. J. Ioannou, "Generalized stability theory. 1. Autonomous operators," J. Atmos. Sci. **53**, 2025 (1996).
[54]B. F. Farrell and P. J. Ioannou, "Perturbation growth and structure in time-dependent flows," J. Atmos. Sci. **56**, 3622 (1999).
[55]B. F. Farrell and P. J. Ioannou, "Transient and asymptotic growth of two-dimensional perturbations in viscous compressible shear flow," Phys. Fluids **12**, 3021 (2000).
[56]R. O. Grigoriev, "Transient growth in driven contact lines," Physica D **209**, 105 (2005).
[57]B. D. Edmonstone, O. K. Matar, and R. V. Craster, "Surfactant-induced fingering phenomena in thin film flow down an inclined plane," Physica D **209**, 62 (2005).
[58]C. M. Bender and S. A. Orszag, *Advanced Mathematical Methods for Scientists and Engineers* (Springer-Verlag, New York, 1999).
[59]P. B. Kahn, *Mathematical Methods for Scientists and Engineers: Linear and Nonlinear Systems* (Dover, New York, 1990).
[60]M. Abramowitz and I. A. Stegun, *Handbook of Mathematical Functions with Formulas, Graphs, and Mathematical Tables* (USGPO, Washington, DC, 1964).
[61]A. H. Nayfeh, *Perturbation Methods* (Wiley Interscience, New York, 1973).